

***Candida* pathogens induce protective mitochondria-associated type I  
interferon signalling and a damage-driven response in vaginal  
epithelial cells**

**Marina Pekmezovic<sup>1\*</sup>, Hrant Hovhannisyan<sup>2,3,9\*</sup>, Mark S. Gresnigt<sup>4</sup>, Elise Iracane<sup>5</sup>, João  
Oliveira-Pacheco<sup>5</sup>, Sofia Siscar-Lewin<sup>1</sup>, Eric Seemann<sup>6</sup>, Britta Qualmann<sup>6</sup>, Till Kalkreuter<sup>1</sup>,  
Sylvia Müller<sup>7</sup>, Thomas Kamradt<sup>7</sup>, Selene Mogavero<sup>1</sup>, Sascha Brunke<sup>1</sup>, Geraldine Butler<sup>5</sup>,  
Toni Gabaldón<sup>2,3,8,9,#</sup>, Bernhard Hube<sup>1,10#</sup>**

1 - Department of Microbial Pathogenicity Mechanisms, Leibniz Institute for Natural Product  
Research and Infection Biology, Hans Knoell Institute, Adolf-Reichwein-Straße 23, 07745, Jena,  
Germany

2 - Bioinformatics and Genomics Programme, Centre for Genomic Regulation (CRG), Barcelona  
Institute of Science and Technology (BIST), Dr. Aiguader 88, 08003 Barcelona, Spain;

3 - Universitat Pompeu Fabra (UPF), 08003 Barcelona, Spain;

4 – Junior Research Group Adaptive Pathogenicity Strategies, Leibniz Institute for Natural Product  
Research and Infection Biology, Hans Knoell Institute, Adolf-Reichwein-Straße 23, 07745, Jena,  
Germany

5 - School of Biomedical and Biomolecular Science and UCD Conway Institute of Biomolecular  
and Biomedical Research, Conway Institute, University College Dublin, Belfield, Dublin, Ireland

6 - Institute for Biochemistry I, Jena University Hospital – Friedrich Schiller University Jena,  
Nonnenplan 2, 07743 Jena, Germany

7 - Institute of Immunology, Universitätsklinikum Jena, Leutragraben 3, 07743 Jena, Germany

8 - Institució Catalana de Recerca i Estudis Avançats (ICREA), Passeig Lluís Companys 23, 08010  
Barcelona, Spain

9 - Current address: Life Sciences Department, Barcelona Supercomputing Center (BSC), Jordi  
Girona, 29, 08034 Barcelona, Spain; Mechanisms of Disease Department, Institute for Research in  
Biomedicine (IRB), Carrer de Baldori Reixac 10, 08028, Barcelona, Spain

10 – Institute of Microbiology, Friedrich Schiller University, Neugasse 24, 07743 Jena, Germany

\* - These authors share equal first authorship

# - These authors share equal senior and corresponding authorship

**Corresponding authors:**

Bernhard Hube: [bernhard.hube@leibniz-hki.de](mailto:bernhard.hube@leibniz-hki.de) ORCID: 0000-0002-6028-0425

Toni Gabaldón: [toni.gabaldon.bcn@gmail.com](mailto:toni.gabaldon.bcn@gmail.com) ORCID: 0000-0003-0019-1735

## Abstract

Vaginal candidiasis is an extremely common disease predominantly caused by four phylogenetically diverse species: *Candida albicans*, *C. glabrata*, *C. parapsilosis*, and *C. tropicalis*. Using a time course infection model of vaginal epithelial cells and dual RNA-Sequencing, we show that these species exhibit distinct pathogenicity patterns, defined by highly species-specific transcriptional profiles during infection of vaginal epithelial cells. In contrast, host cells exhibit a homogeneous response to all species at early stages of infections, which is characterized by sub-lethal mitochondrial signalling inducing a protective type I interferon response. At later stages, the transcriptional response of the host diverges in a species-dependent manner. This divergence is primarily driven by the extent of epithelial damage elicited by species-specific mechanisms such as secretion of the toxin candidalysin by *C. albicans*. Our results uncover a dynamic, biphasic response of vaginal epithelial cells to *Candida* species, characterized by protective mitochondria-associated type I interferon signalling and a species-specific damage-driven response.

## INTRODUCTION

Vulvovaginal candidiasis (VVC) is among the most common fungal infections, affecting 70-75% of women at least once in their lifetime<sup>1</sup>. VVC is characterized by acute inflammation of the vaginal mucosa due to the overgrowth of normally commensal *Candida* species<sup>2-4</sup>. Although *C. albicans* is the predominant cause of VVC, the prevalence of species like *C. glabrata*, *C. parapsilosis*, and *C. tropicalis* has increased (reviewed in<sup>5</sup>). Despite the shared genus name, these species are phylogenetically diverse and often have non-pathogenic close relatives, indicating that their ability to infect humans have emerged independently<sup>6</sup>. How these diverse *Candida* species interact with host cells have rarely been addressed on a comparative basis. Improved knowledge of similarities and species-specific characteristics of infection processes is crucial to understand the pathogenesis, improve diagnostics, and therapy of candidiasis<sup>7</sup>.

Research on host-fungal interactions has been mainly focused on immune cells, which are considered crucial players in the defence against fungal infections<sup>8,9</sup>. However, epithelial cells play a fundamental role in shaping the host defence against fungi, which goes beyond their function as a physical barrier<sup>10-15</sup>.

Studies in infection biology often focus on either the pathogen or the host response, yet microbial pathogenesis can be best interpreted in the framework of dynamic host-microbe interactions. Dual RNA-sequencing (RNA-Seq) enables combined assessment of transcriptional responses of host and pathogen<sup>16,17</sup>, and provides insights into the interactions of fungal pathogens with different host cells<sup>17-23</sup>.

To elucidate general and species-specific interactions between vaginal epithelial cells and the four

most-prevalent VVC-causing *Candida* species, we applied dual RNA-Seq and an *in-vitro* infection model. Our experimental design allows the pathogens to deploy their arsenal of pathogenicity factors without restriction by the immune system. Further, it facilitates specific investigation of epithelial recognition and defence mechanisms, which constitute the first line of defence against infecting fungi.

Our results reveal that fungal transcriptomes show species-specific patterns during infection, likely reflecting the independently evolved pathogenic potential of *Candida* species. Vaginal epithelial cells display a biphasic response: an early protective type I interferon (IFN) response, mediated by sub-lethal mitochondrial signalling, and a damage-associated late response depending on species-specific pathogenicity mechanisms.

## RESULTS

### *Candida* species-specific pathogenicity patterns

To study the interaction of the four most common *Candida* species causing VVC with vaginal epithelial cells, we first assessed their adhesion, invasion, and damage potential as well as growth rates and morphologies (Fig. 1a). Despite similar adhesion rates of all species, only *C. albicans* switched to hyphal growth, invaded epithelial cells, and induced necrotic cell damage. Non-invading *C. glabrata* and *C. tropicalis* cells caused low damage levels. *C. glabrata* grew only in the yeast morphology, whereas occasional pseudohyphae were observed for *C. tropicalis*. Finally, *C. parapsilosis* remained in the yeast morphology during the entire course of infection, forming cell aggregates, but did not invade or caused damage. All species exhibited similar growth rates (Fig. 1b) and showed a biofilm layer 24 hours post-infection (hpi), excluding the possibility that differences in epithelial damage resulted from different proliferation rates (Fig. 1c). These results show species-specific pathogenicity patterns, involving different morphologies, levels of invasion, and damaging capacity.

### Species-specific transcriptional responses to epithelial cells

Subsequently, we investigated whether these differential pathogenicity patterns were reflected in the transcriptional responses of both fungal and epithelial cells (see experimental setup in Extended Data Fig. 1 and cross-mapping analysis between human and yeast sequencing reads in Supplementary files 1-4). The transcriptional dynamics of each *Candida* species throughout the infection was analysed (Fig. 2). All species induced rapid transcriptional responses following infection with increasing numbers of differentially expressed (DE) genes over the course of infection (Fig. 2a, Supplementary files 5-8). Gene Ontology (GO) enrichment analysis revealed the function of DE genes (Fig. 2b, Supplementary file 9). We observed species-specific functional enrichments, albeit with some commonalities. At 3 hpi, *C. albicans* and *C. glabrata* activated

carbohydrate catabolic processes and stress response pathways. *C. parapsilosis* up-regulated, among others, genes related to iron transport, ribosome assembly, and translation. In contrast, *C. tropicalis* DE genes were mainly related to RNA processing, ribosome biogenesis, and ergosterol biosynthetic processes. At later stages, similar functional enrichments were observed across the species. The GO terms oxidation-reduction process, fatty acid beta-oxidation, iron homeostasis, and acetate catabolism, were enriched in at least three species throughout the infection.

When comparing DE genes across species, a remarkably distinct pattern was observed for each pathogen (Extended Data Fig. 2). Analysis of the distribution of species-specific (without orthologs in the other species), partially shared (with orthologs in one or two of the other species) and fully shared (1-to-1 orthologous genes in all species) DE genes (Extended Data Fig. 2a) revealed that species-specific and partially shared genes constitute a substantial proportion (31-72%). Moreover, species-specific genes are more likely to be DE than fully shared genes (Chi-square test  $p < 0.05$ , except for *C. tropicalis*). Even orthologous genes present in all four species showed species-specific differential expression (Extended Data Fig. 2b). Consistently, Principal Component Analysis (PCA) based on orthologous gene expression showed species-specific clusters (Extended Data Fig. 2c).

Gene co-expression analysis was used as an independent approach to investigate commonalities and differences of fungal transcriptional responses. By constructing host-pathogen interaction co-expression networks, highly interconnected gene clusters (modules) were defined and their biological functions were inferred by GO term analysis. In each fungal infection scenario, we detected numerous modules of co-expressed genes (22-28 modules, Supplementary file 10).

Based on fully shared genes, we then assessed whether the fungal genes in the co-expressed modules are conserved across species. Distinct modules were observed for each *Candida* species with few shared genes. On average, only 5% of orthologous genes were shared between any modules of different species (Extended Data Fig. 3). Therefore, the genes in the co-expression modules functionally showed a large species-specificity (Supplementary file 10), with few exceptions. The modules with the highest similarity, i.e. module3 in *C. glabrata* and module3 in *C. tropicalis*, are both enriched for genes associated with DNA replication. Interestingly, we observed modules related to adhesion in *C. albicans* (module11) and *C. tropicalis* (module13), respectively, possibly related to shared virulence features of these two species.

### **Infection-specific DE genes of *Candida* species**

Comparisons of *C. albicans* gene expression during infection of oral epithelium or vascular endothelium, and growth in the tissue culture medium, revealed that only a fraction of genes were specifically expressed during interactions with host cells<sup>20</sup>. This indicates that most of the genes induced during interaction with the host are also required for growth in culture media.

To investigate whether such a phenomenon also occurs during interaction with vaginal cells, controls of fungal cells grown in culture medium only were investigated (Extended Data Fig. 1 and Supplementary table 1). A subtraction of the DE genes in medium from those expressed on epithelial cells revealed a large overlap between the DE genes during infection and in culture medium (Fig. 4 and Supplementary files 5-8). The infection-specific genes are mostly species-specific (Extended Data Fig. 4) and GO enrichment analysis identified different functional enrichments depending on the species (Supplementary file 9).

These were characterized by genes involved in mitochondrial electron transport and ATP synthesis for *C. glabrata*, ergosterol biosynthesis, sulfite and manganese ion transport for *C. parapsilosis*, and ribosome biogenesis and rRNA processing for *C. tropicalis*. No functional enrichments were identified in the up-regulated infection-specific *C. albicans* genes, yet the down-regulated genes showed enrichment in three GO terms related to white-opaque phenotypic switching. These down-regulated genes include *WOR1*, a master regulator inducing the less virulent opaque state<sup>24</sup>.

In summary, distinct transcriptional patterns for each yeast species during infection were observed, suggesting highly species-specific strategies to cope with epithelial cells.

### **Epithelial transcriptomic responses to *Candida* species**

To shed light on how the *Candida* species-specific pathogenicity and transcriptional patterns influenced the host response, epithelial transcriptome responses to infections were analysed (Fig. 3a and b). The epithelial cell transcriptome dynamics show a bias towards up-regulation of genes at the initial stages of infection (Fig. 3a), which is consistent with previous findings<sup>25</sup>.

When compared against the total number of DE genes (Fig. 3c, top panel), the proportion of common DE genes induced by infection with any of the four species decreases throughout the time course – 8.8% of common DE genes at 3 hpi, and 7.6% and 6.4% at 12 hpi and 24 hpi, respectively.

A similar pattern is observed when comparing common DE genes to the DE genes induced specifically by each fungal species (Fig. 3c, bottom panel). The larger fraction of shared DE genes at the early time points suggests that the response to the different yeast species is more conserved at early infection stages while increased species-specificity is observed at later stages (Fig. 3b and 3c).

PCA analysis of the gene expression of epithelial cells revealed a similar pattern (Fig. 3d). The tight clustering at 3 hpi indicates that epithelial cells exhibit a uniform transcriptional response to the four *Candida* species at early stages of infection, in contrast to the fungal transcriptional profiles. However, the epithelial transcriptomes diverge from 12 hpi onwards, and at 24 hpi we observed three distinct clusters of responses to the different species. The transcriptional response of epithelial cells to *C. tropicalis* and *C. glabrata* shows high similarity, being different from the responses to *C. albicans* or *C. parapsilosis*. Functional GO term enrichment analysis revealed a similar trend: at the early time point, GO terms associated with mitochondrial processes are enriched for all species,

and of type I interferon (IFN) responses for all species except *C. tropicalis*. At later stages, species-specific terms appeared (Fig. 3e).

Based on these results, we decided to unravel the basis of the two observed key phenomena: (1) the uniform early transcriptional response related to mitochondria and type I IFN signalling; and (2) the divergence of the host transcriptome response at later stages of infection.

#### **Uniform early responses to *Candida* infections**

The up-regulation of genes associated with the respiratory electron transport chain (Fig. 3e) in epithelial cells at early time points with all *Candida* species included induction of all mitochondrial genes (Fig. 4a). The response was dependent on viable fungi being in direct contact with the epithelial cells (RNA-Seq, Extended Data Fig. 6, Supplementary files 5-8, RT-qPCR, Fig. 4a). Similarly, our co-expression network analysis identified host modules with functional enrichment of mitochondrial genes and oxidative phosphorylation across all infections (Supplementary file 10). These observations suggest that mitochondria-associated processes are triggered in epithelial cells upon infection with *Candida* species.

Host mitochondria have recently been identified as hubs of the innate immune responses<sup>26,27</sup>. In particular, mitochondrial signalling is known to activate type I IFN signalling pathways<sup>28</sup>. We observed enrichment of GO terms (Fig. 3e) and up-regulation of Interferon-Stimulated Genes (ISGs) associated with the type I IFN response<sup>29</sup>, upon exposure of epithelial cells to the four *Candida* species (Fig 4a). Since type I IFN responses are implicated in anti-viral host defence, additional metagenomic analyses were performed, and no viral contamination was detected.

The connection between ISGs expression and mitochondrial functions of the host was characterized during early *Candida* infection. Morphological changes of the mitochondrial network in epithelial cells were observed, changing from reticular (uninfected) to fragmented (infected), and an accumulation of mitochondria around the nucleus (Fig. 4b). Some mitochondria in infected epithelial cells lost their integrity and changed their shape, but not in uninfected cells (Fig. 4c, d). Additionally, endoplasmic reticulum regions were found surrounding these altered mitochondria, suggesting mitophagy of damaged mitochondria. Interestingly, mitochondria were also localized frequently around the invading hyphae of *C. albicans* (Fig. 4c).

Mitochondrial membrane potential ( $\Delta\Psi_m$ ), a key indicator of mitochondrial health, indicated depolarization in epithelial cells infected with any of the four species (Fig. 4e). This change in  $\Delta\Psi_m$  is associated with the production of mitochondrial reactive oxygen species (mtROS), critical players in the regulation of immune signalling pathways<sup>30</sup>. Epithelial mtROS levels were increased upon infection with all four species (Fig. 4f). Finally, release of mitochondrial DNA (mtDNA) into the cytosol was observed during the infection with all *Candida* species (Fig. 4g). The release of mtROS and mtDNA was not detected with killed *C. albicans* cells or when contact was restricted using a

transwell system (Fig. 4e and f). This supports our notion that viable *Candida* cells in direct contact with epithelial cells induce mitochondrial dysfunctions, at both transcriptional and biochemical levels (Fig. 4h).

During infection with bacteria or viruses, host mitochondria can release mtDNA into the cytosol acting as a damage-associated molecular pattern (DAMP) that activates immune pathways<sup>31</sup>. Cytosolic mtDNA can bind the DNA sensor cGAS and promote STING-IRF3-dependent signalling to induce a type I IFN response<sup>28</sup>. In line with this, depletion of epithelial mtDNA (Fig. 5a) prevented up-regulation of ISGs following *Candida* infections (Fig. 5b). In addition, transfection of uninfected epithelial cells with amplified mtDNA induced ISG expression (Fig. 5c). Transfection of uninfected epithelial cells with total DNA from epithelial cells only induced ISGs when the transfected DNA contained mtDNA (Fig. 5d), which supports the role of mtDNA in induction of ISG expression (Fig. 5e).

Although mitochondrial dysfunction is a hallmark of cellular apoptosis, no apoptotic or necrotic epithelial cells were observed during early stages of infections (Extended Data Fig. 5). This was expected since the mitochondrial dysfunctions were only transiently observed. Later during infection, we observed necrotic cell death, but no increase in apoptosis compared to the uninfected control (Extended Data Fig. 5). The A431 cell line lacks functional p53, an important apoptosis inducer<sup>32</sup>. However, we observed similar mitochondrial depolarization in primary vaginal cells upon *Candida* infections, while apoptosis levels did not differ between infected and uninfected cells (Extended Data Fig. 5). Additionally, treatment of A431 cells with the apoptosis inducer staurosporine excluded that the observed mitochondrial signalling and induction of ISG expression were related to apoptosis (Extended Data Fig. 5).

The function of many ISGs remains poorly characterized, but induction is associated with protection against viral infections<sup>33</sup>. To gain insights into their role during *Candida* infection, selected ISGs (*IFI6*, *MX2*, *CMPK2*) were silenced in epithelial cells prior to infection with *C. albicans*. *IFI6* was selected since it was previously observed to be induced by *C. albicans*<sup>34</sup>, *MX2* was among the most highly up-regulated common genes (this study), and *CMPK2* encodes a protein with mitochondrial localization<sup>35</sup>. The level of epithelial damage was increased once these ISGs were silenced (Fig. 6a). While stimulation of cells with IFN- $\beta$  (0.1 ng/ml) prior to infection resulted in reduced damage (Fig. 6b), blocking interferon- $\alpha/\beta$  receptor (IFNAR) signalling led to increased damage (Fig. 6b). These data illustrate that type I IFN signalling increases epithelial resistance to *Candida* infection.

Neutrophil recruitment and activation is a hallmark of vaginal candidiasis<sup>36</sup>. Pro-inflammatory mediators such as IL-6 or IL-1 $\beta$ , characteristic for these events, were not produced during *Candida* infection (Fig. 6c), while IL-1 $\alpha$  and IL-8 levels increased (Fig. 6d), correlating with the level of

245 damage. IL-8 levels also increased upon IFNAR blocking (Fig. 6d), suggesting a relationship  
246 between epithelial type I IFN signalling and the initiation of pro-inflammatory responses, which can  
247 drive immunopathology in VVC.

248 When exposing neutrophils to culture supernatants of epithelial cells infected with *Candida* species,  
249 IL-8 release was observed (Fig. 6e). IL-8 levels further increased when the IFNAR receptor was  
250 blocked in the same setting (Fig. 6e). This suggests that type I IFN signalling in epithelial cells  
251 restricts pro-inflammatory responses and subsequent neutrophil activation (Fig. 6f).

## 252 **Damage-driven transcriptional responses**

253 While the initial phases of infection showed a conserved epithelial response, this response separated  
254 into different trajectories at later stages. Considering that host cell damage is a major determinant of  
255 pathogenicity<sup>37-39</sup>, we hypothesized that *Candida* species-specific differences in the damaging  
256 potential (Fig. 1, Extended Data Fig. 6), reflected by the pattern observed in the PCA plot (Fig. 3d),  
257 drive the different transcriptional responses during late infection.

258 Epithelial cell damage during *C. albicans* infection is mediated by the cytolytic toxin candidalysin  
259<sup>40,41</sup>. Deletion of the gene *ECE1*, encoding candidalysin, renders *C. albicans* almost unable to inflict  
260 damage to epithelial cells, despite normal growth, adhesion, filamentation, and invasion properties  
261<sup>25,40</sup>.

262 To determine whether candidalysin-driven epithelial cell damage might dictate the transcriptional  
263 response of epithelial cells, the transcriptional response upon interaction with the *C. albicans*  
264 *ece1Δ/Δ* mutant was investigated. The epithelial transcriptional response to the candidalysin-  
265 deficient mutant was notably similar to the response to the non-damaging species *C. parapsilosis*  
266 (Extended Data Fig. 6 and 7). This confirms a pivotal role for host-cell damage as the major driver  
267 of epithelial transcriptional responses to *Candida* infections. GO term enrichment analysis of 774  
268 genes, specifically up-regulated upon the exposure to damaging *C. albicans* wild type, showed no  
269 significant enrichment for any process. However, previous studies demonstrated that candidalysin  
270 induces c-Fos and mitogen-activated protein kinase (MAPK) driven release of the proinflammatory  
271 cytokines IL-1α, IL-1β and the chemokine IL-8 in vaginal epithelial cells<sup>12,25</sup>. Manual inspection  
272 revealed similar responses including up-regulation of *HBEGF*, *CXCL1*, *CXCL2*, *IL1A*, *IL1B*,  
273 *CXCL8*, and *CSF2* and genes associated with the “danger”-response pathway *FOS*, *JUN*, and  
274 *DUSP1*<sup>12,25</sup>. This confirms that epithelial damage and proinflammatory signals that drive neutrophil  
275 recruitment induced by *C. albicans* depend almost exclusively on candidalysin.

## 277 **DISCUSSION**

278 Here we dissected the interaction of the main four *Candida* species that cause VVC with human  
279 vaginal epithelial cells. Large-scale dual transcriptomic analysis of human and fungal cells during

the course of infection revealed common and species-specific *Candida* pathogenicity patterns. We observed a biphasic host response to *Candida* species, characterized by an early common mitochondria-induced type I IFN signalling and diverged responses at later stages depending on the species-specific capacities to inflict damage to the vaginal epithelial cells.

It has previously been hypothesized that phylogenetically diverse *Candida* species independently acquired their ability to colonize and infect humans and thus are expected to use distinct sets of pathogenicity mechanisms<sup>6,23</sup>. Our study empirically supports this hypothesis by showing that the main VVC pathogens express species-specific transcriptional responses and pathogenicity patterns upon contact with vaginal epithelial cells, even when only orthologous genes were considered.

Similarly, the epithelial transcriptional responses at late stages of infection were specific depending on the *Candida* species. These diverse patterns paralleled the varying damaging capacities of the four *Candida* species. We confirmed fungal-induced damage as the major driver of epithelial responses by infecting epithelial cells with the non-damaging candidalysin-deficient *C. albicans* *ece1Δ/Δ* mutant. The epithelial transcriptional response to this mutant did not resemble the response to wildtype *C. albicans*, but instead was similar to the response to the non-damaging species *C. parapsilosis* at late stages of infection. This finding confirms the crucial role of candidalysin during interaction of *C. albicans* with vaginal epithelial cells leading to DAMP release that can catalyse immunopathology during vaginal infections<sup>25</sup>.

In contrast, the epithelial response towards the different *Candida* species was highly uniform at early stages. This initial response was driven by common epithelial processes rather than by convergent activities (such as virulence programs) of the tested *Candida* species. For example, independent of their viability, *DOCK8* expression was up-regulated following infection with any of the four *Candida* species (Supplementary files 5-8). Although *DOCK8* has multiple signalling functions, it was suggested to promote immune responses to diverse external stimuli<sup>42</sup>. Several studies associated *DOCK8* with mucocutaneous candidiasis due to impaired Th17 differentiation<sup>43-45</sup>. Thus, it is tempting to speculate that *DOCK8* may regulate the recognition of *Candida* species by epithelial cells.

Mitochondria-encoded genes and genes associated with the type I IFN response pathway were uniformly up-regulated. While type I IFN responses are associated with viral infections<sup>46</sup>, type I IFN responses have been observed in peripheral blood mononuclear cells infected with *C. albicans*<sup>34</sup>. Additionally, type I IFN responses were recently shown to dysregulate host iron homeostasis and enhance *C. glabrata* infection<sup>47</sup>, and the type I IFN-inducing RIGI helicase MDA5 has been associated with systemic as well as chronic mucocutaneous candidiasis<sup>48</sup>. Finally, IFNαR1 signalling is crucial for efficient host defence against systemic candidiasis in mice<sup>49</sup>.

Our data show that type I IFN signalling, induced by vaginal epithelial cells in response to *Candida*

species, increases epithelial resistance to infection and dampens pro-inflammatory responses. Such an immune response may be relevant in host niches colonized by commensal microbes that need to be tolerated without induction of inflammation. For example, intestinal epithelial cells regulate the durability and specificity of immune responses and guide the immune system to differentiate between commensal and pathogenic microbiota *via* expression of type I IFN and ISGs<sup>50-52</sup>. Since *Candida* species are commensals of the vaginal mucosa<sup>53</sup>, the epithelial type I IFN pathway may maintain the threshold between commensalism and pathogenicity and regulates antifungal immunity. Our results show a protective role for ISGs and IFNAR signalling in increasing epithelial resistance to *Candida*-induced damage while reducing potentially detrimental proinflammatory responses. Supporting this, Li *et al.* showed that administration of human IFN $\alpha$ -2b decreased the inflammation and vaginal epithelial damage in a rat VVC model<sup>54</sup>. The combined effects, immunomodulation and epithelial antifungal resistance, may be crucial to restrict *Candida* species to commensalism and avoid inflammation-driven pathology. Moreover, this highlights the type I IFN response as a potential target for host-directed therapy aimed at improving epithelial resistance and prevention immunopathology. Such a therapy could benefit VVC patients that fail to recover with antifungal treatment alone, a phenomenon often observed in women with recurrent VVC<sup>55</sup>.

At the early infection stage also genes encoded by mitochondrial DNA, in particular genes coding for the respiratory electron-transport chain, were up-regulated. Apart from the well-established roles in metabolism and energy production, mitochondria are central hubs in innate immunity<sup>26,27</sup>. Mitochondrial dysfunction, resulting in mtROS and mtDNA release into the cytosol, can act as a DAMP and activate various signalling pathways<sup>26-28,56-58</sup>, including induction of cytokine production<sup>59</sup> and type I IFN responses<sup>60</sup>. Intriguingly, altered mitochondrial function at early stages of infection were observed in different host cell types upon infections with various bacterial pathogens<sup>61-64</sup>, including *Chlamydia trachomatis*<sup>65</sup>, *C. pneumoniae*<sup>66</sup>, *Listeria monocytogenes*<sup>67</sup>, and the parasite *Toxoplasma gondii*<sup>68</sup>. These mechanisms have, however, not yet been observed during fungal infections. We observed that mitochondria in *Candida*-infected vaginal epithelial cells changed shape and lost integrity, had decreased membrane potential, and released mtROS and mtDNA. The release of mtDNA was observed to act as a DAMP that activates the type I IFN pathway during *Candida* infections of the vaginal epithelia. This activation may potentially occur through the STING-pathway, as shown previously for *Streptococcus pneumoniae*<sup>69</sup>, on the level of post-translational modifications<sup>70</sup>.

To maintain epithelial integrity and mount an effective epithelial host defence while preventing detrimental inflammatory responses, such a mitochondrial response must occur on a sub-lethal level<sup>59</sup>. Accordingly, no changes in apoptosis were observed over the course of infection. The non-lethal

mitochondrial dysfunction was also independent of necrosis, which was only observed at later stages. Likewise, we observed consistent activation of the type I IFN pathway, which is suppressed by apoptotic caspases<sup>71</sup>. Consequently, induction of apoptosis abrogated expression of ISGs. Similar studies with *L. monocytogenes* and *T. gondii* showed that mitochondrial dysfunction was uncoupled from the apoptotic pathway<sup>67,68</sup>. During infection of epithelial cells with diverse microbes, the mitochondrial apoptosis apparatus can be activated at a low level, which is insufficient to induce apoptosis<sup>59,72</sup>. This phenomenon has been termed limited mitochondrial outer membrane permeabilization, or “minority MOMP”, and induces pro-inflammatory cytokine production *via* STING.

Viruses, bacteria, and parasites all can induce minority MOMP, thereby contributing to cytokine release during infection<sup>59</sup>. We propose that this mechanism plays a significant role in epithelial sensing of *Candida* species, induction of epithelial antifungal immunity, and modulation of immune responses *via* type I IFN signalling.

It remains to be determined how *Candida* species initiate the mitochondrial-induced epithelial type I IFN response. We observed mitochondrial signaling at stages when *C. albicans* has not yet invaded or damaged the epithelial cells, whereas all other *Candida* species failed to invade epithelial cells. We therefore propose that the induction of mitochondrial signaling may rely on sensing of pathogen-associated molecular patterns.

In summary, we identified species-specific pathogenicity patterns of *Candida* species infecting vaginal epithelial cells, which are reflected on the transcriptional level during the course of infection. In contrast, vaginal epithelial cells exhibit a conserved response at early stages, but a diverse, damage-driven response at later stages. The conserved response was characterized by non-lethal mitochondrial signalling, which induced a type I IFN response that protects against *Candida*-induced damage and modulates proinflammatory responses. This acts as a common pathway of host-pathogen interactions between vaginal epithelial cells and *Candida* pathogens.

## **MATERIALS AND METHODS**

### **Fungal strains and culture conditions**

*C. albicans* SC5314<sup>73</sup>, *Candida glabrata* ATCC® 2001™ (obtained from the American Type Culture Collection; ATCC), *C. tropicalis* DSM 4959 (obtained from the German Collection of Microorganisms and Cell Cultures; DSMZ), *C. parapsilosis* 73-037<sup>74</sup> and *C. albicans ece1Δ/Δ*<sup>40</sup> were used in this study. For all experiments, single colonies were picked from Yeast Extract Peptone Dextrose (YPD) agar plates and grown overnight in liquid YPD medium in an orbital shaker at 180 rpm at 30 °C (*C. albicans*, *C. tropicalis*, and *C. parapsilosis*) or 37 °C (*C. glabrata*). Yeast cells were then harvested by centrifugation (20,000 g, 1 min), washed twice with phosphate-

buffered saline (PBS), and adjusted to  $2 \times 10^6$  yeast cells  $\text{ml}^{-1}$ .

#### ***In vitro* vaginal epithelial infection model**

To mimic the vaginal epithelium, A431 epithelial cells (ECs; DSMZ no. ACC 91) were used. These cells are derived from a vulva epidermoid carcinoma and routinely used to model the vaginal mucosa<sup>75,76</sup>. A431 cells were authenticated using STR analysis (DNA fingerprinting) and routinely tested for the absence of mycoplasma contamination. ECs were cultivated in RPMI-1640 medium (ThermoFisher Scientific) supplemented with 10% fetal calf serum (FCS, Bio&Sell) in a humidified incubator at 37°C, 5% CO<sub>2</sub>. For infection, ECs were seeded in 6-well plates ( $3 \times 10^5$  cells per well) and cultured for 2 days. On the day of infection, media in each well was replaced with 1.5 ml RPMI-1640 without FCS and incubated for 30 min in order to allow cells to adjust to the change of medium. In subsequent bioinformatics analyses, we considered the control samples at 30 min in this medium as the 0 h time point. ECs were subsequently infected with *Candida* cells (1.5 ml of  $2 \times 10^6$  yeast  $\text{ml}^{-1}$  in RPMI-1640 without FCS) and incubated at 37°C, 5% CO<sub>2</sub>. Samples for RNA isolation were collected at different time points: 3, 12, and 24 hours post-infection (hpi). More specifically, the well content was removed and replaced with 500  $\mu\text{l}$  of RNeasy Lysis (RLT) buffer (Qiagen), containing 1%  $\beta$ -mercaptoethanol (Roth). Cells were detached using a cell scraper ( $< 3$  min), immediately shock-frozen in liquid nitrogen, and stored at -80°C until further use (see “RNA isolation”). As controls, *Candida* cells alone and ECs alone were incubated for 30 min (0 h control: C0) and 24 hours (24 h control: C24) and samples for RNA isolation were collected as described above.

#### **RNA isolation and pooling**

Collected samples were defrosted on ice and centrifuged for 10 min (20,000 g, 4°C). The supernatant was transferred to a new microcentrifuge tube and used to isolate human RNA (RNeasy Mini Kit, Qiagen), according to the manufacturer's instructions. Fungal RNA was isolated from the pellet, using a freezing-thawing method, as described previously<sup>77</sup>. Both human and fungal RNA concentrations were quantified using a NanoDrop 1000 Spectrophotometer (ThermoFisher Scientific) and RNA quality was assessed with an Agilent 2100 Bioanalyzer (Agilent Technologies). To subsequently achieve sufficient sequencing depth of both counterparts for a robust differential gene expression analysis<sup>78</sup>, corresponding fungal and human RNA samples were then pooled in a 2:3 ratio by weight for further library preparation and sequencing. Before the pooling, we first checked whether this strategy will result in ambiguous read mappings between the host and pathogen data after sequencing and data analysis. To assess the rates of cross-mapping, i.e. reads originated from human but mapped to fungi and vice-versa, which can bias expression level quantifications, we used Crossmapper v. 1.1.0<sup>95</sup> which simulates reads from multiple reference genomes/transcriptomes, maps the data back to the concatenated reference sequences and reports

the rates of cross-mapping. We used the "RNA" mode of Crossmapper and simulated and back-mapped 20 and 40 million 2x50 and 2x75 reads for each fungal species and human, respectively. In all cases, the pooling and sequencing strategy resulted in virtually no cross-mapping between human and yeast data (Supplementary files 1-4).

#### **Growth curves**

*Candida* cells were adjusted to yeast  $\text{ml}^{-1}$  either in YPD or in RPMI medium. Growth was monitored in 96-well-plates by measuring the absorbance at 600 nm every 30 min for 24 hours at 37°C in a microplate reader (Tecan M-Plex). Prior to each measurement plates underwent ten seconds orbital shaking followed by ten seconds waiting time. The  $\text{OD}_{600}$  values were converted into  $\log_2$  and the generation time was calculated from the slope of the exponential growth phase. The experiment was repeated five times (n=5).

#### **UV killing of *Candida***

*Candida* cells from overnight cultures were collected by centrifugation, washed twice with PBS and adjusted to approximately  $5 \times 10^7$  yeast  $\text{ml}^{-1}$  in PBS. The suspension was transferred to a Petri dish as a thin liquid layer (10 ml) and exposed to 4 doses of 100-120 mJ per  $\text{cm}^2$  in a UV-crosslinker (CL 508 S, Uvitec, Cambridge). The efficiency of UV killing was evaluated by plating 50  $\mu\text{l}$  of the sample onto YPD agar and incubated for 48 h at 30°C.

#### **Adhesion assay**

ECs were infected with *Candida* yeast cells as described above and incubated for 1 hour. Non-adherent *Candida* cells were removed by rinsing with PBS. Subsequently, ECs with adhered *Candida* were fixed with Roti®-Histofix 4 % (Roth). Adherent *Candida* cells were stained with Alexa Fluor 647 conjugate of succinylated concanavalin A (ConA; Invitrogen) and visualized using a fluorescence microscope (Leica DM5500B, Leica DFC360 FX). Pictures of each sample were taken until a total of 100 adherent cells were counted. Adhesion was calculated based on the average of *Candida* cells counted in each picture with a defined area. This number was expressed as a percentage of adhered cells versus inoculated cells<sup>77</sup>.

#### **Invasion assay and hyphal length**

ECs were infected with *Candida* cells as described above and incubated for 3 h. Non-adherent *Candida* cells were removed by rinsing with PBS and samples were fixed with Roti®-Histofix 4 %. Extracellular, non-invasive fungal components were stained by ConA. After rinsing with PBS, ECs were permeabilized in 0.5% Triton X-100 for 10 min. Next, fungal cells were stained with Calcofluor white (CFW; Sigma-Aldrich) and visualized by fluorescence microscopy. The total hyphal length was noted, as well as the percentage of invasive hyphae (only CFW-stained), counted from at least 100 hyphae per strain for each biological replicate.

#### **Epithelial damage assay**

ECs were infected with *Candida* cells as described above and incubated for 24 h. Release of the cytoplasmic enzyme lactate dehydrogenase (LDH) was measured as a marker for necrotic epithelial damage<sup>79</sup> using a Cytotoxicity Detection Kit (Roche) according to the manufacturer's instructions. The background LDH value of uninfected ECs (low control) was subtracted, and the corrected LDH release was expressed as % of high (full lysis) control (maximum LDH release induced by the addition of 0.25% Triton X-100 to uninfected ECs for 5 min) unless otherwise stated. For the protection effect experiments, 0.1 ng ml<sup>-1</sup> of interferon-beta (IFN- $\beta$ ; Invivogen) or neutralizing anti-human IFNAR2 antibody (4 ng ml<sup>-1</sup>, PBL Interferon Source, Piscataway, USA) were added to ECs three hours prior to infection.

#### **Transwell assay**

ECs were seeded in 24-well plates (1 $\times$ 10<sup>5</sup> cells per well) in RPMI-1640 with FCS and incubated for two days at 37°C and 5% CO<sub>2</sub>. After medium exchange with 750  $\mu$ l of RPMI-1640 without FCS, transwell inserts (polycarbonate membrane inserts with 0.4 $\mu$ m pore size; Corning), loaded with 250  $\mu$ l of *Candida* suspension (4 $\times$ 10<sup>6</sup> yeast ml<sup>-1</sup>), were placed in the wells. After three hours of incubation, the inserts were discarded and human RNA samples were collected and isolated as described above.

#### **Reverse transcription-quantitative PCR (RT-qPCR)**

Isolated RNA (500 ng) was treated with DNase I (Fermentas) following the manufacturer's recommendations and subsequently transcribed into cDNA using 0.5  $\mu$ g Oligo(dT)12-18 Primer, 200 U Superscript<sup>TM</sup> III Reverse Transcriptase and 40 U RNaseOUT<sup>TM</sup> Recombinant RNase Inhibitor (Thermo Fischer Scientific). Obtained cDNA was diluted 1:5 and used for qPCR with GoTaq<sup>®</sup> qPCR Master Mix (Promega) in a CFX96 thermocycler (Bio-Rad). The expression levels were normalized against beta-actin or 18s rRNA. All primers used are listed in Supplementary table 2.

#### **Measurement of EC mitochondrial DNA (mtDNA) release**

The release of mtDNA in response to infection was measured using the protocol of Bronner and O'Riordan<sup>80</sup> with some modifications. Briefly, ECs were seeded in 6-well plates and infected as described above. After 6 h of infection, the medium and non-adherent *Candida* cells were removed. After addition of 200  $\mu$ l of the cell membrane detergent Igepal CA-630 (1%, NP-40; Sigma-Aldrich), cells were loosened by scraping. Lysates were incubated on ice for 15 min and centrifuged (12,000 g, 15 min, 4 °C). The supernatant was used to isolate human mtDNA from the cytosolic fraction using the DNeasy Blood & Tissue Kit (Qiagen), according to the manufacturer's instructions. Finally, cytosolic human mtDNA was measured by qPCR using 18s rRNA as a reference<sup>80</sup>. Results are presented relative to an uninfected control. Tunicamycin (10  $\mu$ M; Sigma-Aldrich) was used as a positive control, as ER-stress inducer that leads to mitochondrial dysfunction

<sup>81</sup>. The same procedure was carried out on yeast cells only to exclude that fungal cells would also release mtDNA following this protocol. The lysis step did not cause any lysis of yeast cells and no DNA was detected after the isolation procedure, confirming that the DNA obtained from the infected ECs originated from epithelial cells only.

#### **Measurement of EC mitochondrial membrane potential ( $\Delta\Psi_m$ )**

Mitochondrial membrane potential ( $\Delta\Psi_m$ ) was assessed using the dye MitoTracker® Deep Red FM (ThermoFisher Scientific, Ex/Em=644/665 nm). ECs were seeded and infected in 6-well plates and stained with 20nM MitoTracker® Deep Red FM for 15 min at 37°C. ECs were then detached using Accutase®, fixed with Roti®-Histofix 4%. The fluorescence was quantified by flow cytometry (BD FACS Verse®, BD Biosciences, Franklin Lakes, USA), counting 10,000 events; and the data was collected using BD FACSuite v1.0.6.5230 software and analysed using FlowJo v10.2. Carbonyl cyanide 3-chlorophenylhydrazone (CCCP), a protonophore causing mitochondrial depolarization, was used as a positive control (100  $\mu$ M).

#### **EC mitochondrial reactive oxygen species (mtROS) detection**

Production of mtROS was measured using a Mitochondrial Reactive Oxygen Species Detection Assay Kit (Cayman Chemicals). ECs were seeded and infected in a black clear-bottom 96-well plate and measurement of mtROS production of infected and uninfected cells was done at 1 hpi, according to the manufacturer's instructions. Antimycin A (100  $\mu$ M), inducing superoxide radicals leakage from mitochondria, was used as a positive control.

#### **RNA-interference assay**

RNA-interference assay was used to silence the expression of selected ISGs (*IFI6*, *MX2*, and *CMPK2*). Small interfering (si)RNA, control siRNA (siRNA-A; sc-37007), siRNA transfection reagent, and siRNA transfection medium were purchased from Santa Cruz Biotechnology. ECs were seeded in a 6-well plate and transfected with 1  $\mu$ g siRNA according to the manufacturer's instructions. After 48h, cells were infected with *C. albicans*, and 3 hpi, RNA was isolated and silencing of selected genes was confirmed using RT-qPCR. LDH release was measured 24 hpi.

#### **mtDNA depletion assay**

ECs were seeded in 6-well plates and incubated for 2 days. Once confluent, 200  $\mu$ M of 2',3'-dideoxycytidine (ddC; Jena Bioscience) was added to the medium and ECs were incubated for 6 days. mtDNA depletion was confirmed by quantifying mtDNA using qPCR, as described above.

#### **Transfection of ECs**

MtDNA was PCR-amplified from the entire human mitochondrial genome in 17 overlapping fragments as described previously <sup>82</sup>. ECs were transfected with amplified mtDNA fragments (Fig. 5c) or total DNA isolated from ECs with and without their mtDNA depleted (Fig. 5d). Total DNA was isolated using the DNeasy Blood & Tissue Kit (Qiagen). A total of 2  $\mu$ g ml<sup>-1</sup> of DNA was used

to transfect ECs using UltraCruz® Transfection Reagent (Santa Cruz) according to the manufacturer's instructions. After 6 h, RNA samples were collected and the expression of ISGs was quantified by RT-qPCR.

#### **Apoptosis/necrosis assay**

ECs were seeded in black 96-well plates and infected with *Candida* cells as described above. At 3 and 24 hpi, ECs were stained for apoptotic (Apopxin Green Indicator, Ex/Em = 490/525 nm), necrotic (7-aminoactinomycin D, Ex/Em = 546/647 nm) and healthy cells (CytoCalcein Violet 450, Ex/Em = 405/450 nm), using the Apoptosis/Necrosis Assay Kit (Abcam). The fluorescence was measured in a microplate reader (Tecan M-Plex). Staurosporine (1.2 µM; Sigma) was used as a positive control, while uninfected ECs were used as a negative control.

#### **Apoptosis induction**

ECs were seeded in 96-well plates and infected with *Candida* as described above, with the addition of staurosporine (1.2 µM) simultaneously with infection. After 6 h, RNA samples were collected and the expression of ISGs was quantified by RT-qPCR. Results were compared to infected cells incubated in the media without staurosporine.

#### **Collection of EC supernatants**

ECs were infected with *Candida* cells as described above and incubated for 24 h, in the presence or absence of neutralizing anti-human IFNAR2 antibody. Supernatants were collected and stored at -80 °C until use (see Cytokine release and Neutrophil stimulation). Supernatants of only *Candida* cells grown in absence of ECs were included as control.

#### **Cytokine release**

ECs were infected with *Candida* cells as described above and incubated for 24 h. The release of interleukin(IL)-6, IL-8, IL-1α and IL-1β was measured by commercially available human enzyme-linked immunosorbent assay (ELISA) kits (IL-6, IL-8, IL-1β: Invitrogen; IL-1α: R&DSYSTEMS) according to the manufacturer's instructions.

#### **Blood donors**

Human peripheral blood was collected from healthy volunteers (n=3) with ethics approval and after obtaining written informed consent. This study was conducted according to the principles expressed in the Declaration of Helsinki. The blood donation protocol and use of blood for this study were approved by the institutional ethics committee of the University Hospital Jena (permission number 2207-01/08).

#### **Neutrophil cytokine production**

Primary human neutrophils were isolated from blood using a previously published protocol<sup>83</sup> and seeded in a 24-well plate ( $5 \times 10^5$  cells ml<sup>-1</sup>). Neutrophils were exposed for 24 h to supernatants of ECs that had been infected with each of the *Candida* species (24 hpi) to determine whether pro-

inflammatory mediators released by ECs play a role in neutrophil stimulation. Control supernatants of *Candida* cells alone were included to ensure that the neutrophils respond to secretions of the epithelial cells rather than the fungus (blue bars on Fig. 6e). After incubation cytokine release was measured using ELISA as described above.

#### **Fluorescence microscopy**

ECs were seeded in  $\mu$ -Slide 8 Well (ibidi) and infected with *Candida* cells as described above. At 1 hpi, ECs were stained with 100nM MitoTracker® Deep Red FM for 15 min at 37°C, washed and fixed with Roti®-Histofix 4 %. Fluorescent imaging was done using the Cell Observer microscope (Carl Zeiss) with fluorescence settings at 644/665 nm. CCCP was used as a positive control (100  $\mu$ M). Image acquisition was done in a fully blinded manner, to avoid potential bias.

#### **Transmission electron microscopy (TEM) and imaging**

The cells were fixed by adding glutaraldehyde (2.5 % (v/v) final) to the growth medium. After 1 h the cell layer was gently scraped off the surface, collected as a pellet by centrifuging at 600 g, and washed 3 $\times$  with PBS. After fixation in osmiumtetroxide (1% (w/v) in aqua dest.) for 1 h, dehydration in ascending ethanol series with post-staining in uranylacetate was performed. Afterwards the samples were embedded in epoxy resin (Araldite) and ultrathin sectioned (60 nm) using an ultramicrotome Leica Ultracut E (Leica, Wetzlar, Germany). After mounting on filmed Cu grids and post-staining with lead citrate the sections were studied in a transmission electron microscope (EM 902A, Zeiss, Oberkochen, Germany) at 80 kV. Images were acquired with a 1k FastScan CCD camera (TVIPS, München). Mitochondrial aspect ratio (the ratio of length/width) was measured using ImageJ by analyzing at least 80 mitochondria for each condition<sup>84</sup> in one biological replicate. Irregular structures were excluded from analysis. All TEM analyses were conducted in a fully blinded manner, to avoid potential bias in image acquisition and analyses.

#### **Primary vaginal cells**

Primary human vaginal ECs (ATCC® PCS-480-010™) were obtained from ATCC and cultured in Vaginal Epithelial Cell Basal Medium (ATCC® PCS-480-030™), supplemented with components from the “Vaginal Epithelial Cell Growth Kit” (ATCC® PCS-480-040™). The cells were not authenticated, but they were routinely checked for the absence of mycoplasma contamination. Apoptosis/necrosis and mitochondrial membrane potential assay were performed as described for A431 cells.

#### **RNA-Seq library preparation and sequencing**

Library preparation for RNA-Seq was performed with the TruSeq Stranded mRNA Sample Prep Kit v2 (ref. RS-122-2101/2, Illumina) according to the manufacturer's instructions unless specified otherwise. One  $\mu$ g of total RNA was used for poly(A)-mRNA selection using streptavidin-coated

magnetic beads. Samples were then fragmented to ~300bp and subsequently, cDNA was synthesized using reverse transcriptase (SuperScript II, Invitrogen) and random primers. The second strand of the cDNA incorporated dUTP in place of dTTP. Double-stranded DNA was further used for library preparation. It was subjected to A-tailing and ligation of the barcoded Truseq adapters. All purification steps were done using AMPure XP beads (Agencourt). Library amplification was performed by PCR on the size selected fragments using the primer cocktail supplied in the kit. Final libraries were analyzed using Agilent DNA 1000 chip (Agilent) to estimate the quantity and check fragment size distribution and were then quantified by qPCR using the KAPA Library Quantification Kit (KapaBiosystems) before amplification with Illumina's cBot. To avoid potential batch effects, all samples were randomly distributed on the sequencing flowcells. Libraries were sequenced with 2x50 (n=21), 2x75 (n=70) and 2x150 (n=1) read lengths on Illumina's HiSeq 2500 (2x50 bp) and HiSeq 3000 (the rest) at the Genomics Unit of the Centre for Genomic Regulation, Barcelona, Spain. Samples that contained mixed fungal and human RNA were sequenced for (on average) ~65 million reads (see Supplementary table 1 and Extended Data Fig. 1 for details) in order to achieve sufficient sequencing depth for robust downstream analysis<sup>78</sup>.

#### **Bioinformatics data analysis**

FastQC v. 0.11.6<sup>85</sup> and Multiqc v. 1.0<sup>86</sup> were used to perform quality control of raw sequencing data. Read trimming, when necessary, was performed by Trimmomatic v. 0.36<sup>87</sup> with TruSeq3 adapters using 2:30:10 parameters and discarding reads shorter than sequenced read length.

For read mapping and quantification, we used splice-junction sensitive read mapper STAR v. 2.5.2b<sup>88</sup> using basic two-pass mode and default parameters. For samples comprising either fungal or human RNA, reads were mapped to the corresponding reference genomes. In the case of pooled samples containing RNA from both the host and the pathogen, the data were mapped to concatenated human and corresponding yeast reference genomes. For human data, we used the primary genome assembly GRCh38 and genome annotations from Ensembl database release 89 (last accessed on 8 of August 2017)<sup>89</sup>. Reference genomes and genome annotations for *C. albicans* SC5314 (assembly 22), *C. glabrata* CBS138 and *C. parapsilosis* CDC317 were obtained from *Candida* Genome Database (CGD, last accessed on 17 of August 2017,<sup>90</sup>). From the phased reference genome and annotations of *C. albicans*, we selected Haplotype A to perform further analysis in order to avoid substantial rates of ambiguously mapped reads. Reference sequence and annotations for *C. tropicalis* were obtained from RefSeq database (last accessed on 9 of August 2017,<sup>91</sup>). The genes missing from RefSeq genome annotations were manually added from CGOB database<sup>92</sup>. GFF genome annotation files were converted to GTF format using gffread utility v. 0.9.8<sup>93</sup>. We used Centrifuge v. 1.0.4<sup>94</sup> to test the presence of viral contamination in our dataset, by remapping the reads that did map neither to human nor fungal reference genomes to the whole

NCBI nt database (downloaded on the 23rd of March 2018). No traces of contamination were observed.

Differential gene expression analysis was performed using the Bioconductor package DESeq2 v. 1.26.0<sup>96</sup> using read counts obtained by STAR mapping. For human samples and each fungal species, we compared time point 0 with other time points throughout the course of infection by Wald test using the *contrast* option of DESeq2. To detect any statistically significant changes of expression throughout the course of infection, we also used a likelihood ratio test of DESeq2, by dropping the "time" component of the formula design. Genes with  $|\log_2 \text{fold change}| > 1.5$  and adjusted  $p$ -value ( $p_{\text{adj}}$ )  $< 0.01$  were considered DE, unless specified otherwise. To account for possible batch effects in the experiments involving *C. albicans ece1Δ/Δ* and non-viable fungal cells, we applied RUVg function of RUVseq v1.20<sup>97</sup> Bioconductor package, using non-DE genes (basemean  $> 10$  and  $p_{\text{adj}} > 0.05$  obtained by likelihood ratio test in DESeq2) across all samples and time points as negative controls. Since the optimal parameters for the batch effect removal algorithm are not defined in prior, we employed a strategy of incremental increase of  $k$  values ( $k=1,2,\dots,n$ ), until we observed disruption of the PCA clustering of original data from the first batch of sequencing. To perform differential expression analysis, the obtained matrix of batch effect coefficients was further supplied to the design formula of DESeq2 object, which was subsequently run using original count data. For plotting "batch-free" PCA plots, we used batch-corrected counts retrieved from RUV package.

The list of 1-to-1 orthologs between the four fungal species was obtained from CGD. For interspecies gene expression comparisons, the raw read counts for each fungal species were normalized by gene length and library size. Gene Ontology (GO) term enrichment analysis was performed using clusterProfiler package v. 3.14.3<sup>98</sup>. GO enrichment plots were produced with *dotplot* function using *showCategory* set to 10 (for human data) and 8 (for fungal data) for better plot readability (the full list of GO enrichments is available in Supplementary file 9). Adjustment of  $p$ -values was done by Benjamini-Hochberg procedure. GO information for fungal species was obtained from CGD, while for human data we used "Genome-wide annotation for Human database" (org.Hs.eg.db) v. 3.10.0 in R<sup>99</sup>.

We assessed the patterns of host-pathogen gene co-expression across the infections using the weighted correlation network analysis approach implemented in WGCNA v. 1.69<sup>100</sup>. For each infection, we combined fungal and corresponding human data at all available time points of infection, excluding the data of *C. albicans ece1Δ/Δ* mutant. As recommended by package developers, we selected genes that had 10 or more counts in more than 90% of samples for downstream analysis. As expression levels, we used variance stabilized read count data, obtained by *vst* function of DESeq2. Before the actual network construction, first we selected the  $\beta$  power

values using the *pickSoftThreshold* function implying an unsigned network. The minimum  $\beta$  values reaching 80% of scale-free network topology, namely 12, 20, 7 and 22 for infections with *C. albicans*, *C. glabrata*, *C. parapsilosis* and *C. tropicalis*, respectively, were used for downstream analysis. After network construction, we inferred modules (i.e. highly interconnected clusters of genes) in the WGCNA networks using 1-Topology Overlap Matrix values at 0.25 hclust tree cutoff, and identified eigengenes (i.e. the first principal component of each module). For each identified module, we performed GO term enrichment analysis of fungal and host genes using clusterProfiler (Supplementary file 10), selecting top 3 enrichments with the lowest adjusted *p*-values. Then, fungal gene content of each module of a given fungal species was compared against those of all modules of other three species taking into account 1-to-1 orthology information (Extended Data Fig. 3). This analysis was done for modules, which contained at least one fungal gene. Similarity between fungal gene contents of two given modules was defined as intersection of fungal gene lists of these modules divided by the union of these gene lists.

All custom calculations and visualizations were performed in R v. 3.6.1 using various packages (all the packages and their versions are available at our GitHub page [https://github.com/Gabaldonlab/Host-pathogen\\_interactions](https://github.com/Gabaldonlab/Host-pathogen_interactions)).

### Statistics and Reproducibility

Experiments were performed in biological triplicates ( $n=3$ ) with three different donors (neutrophil cytokine release) or three independent experiments. Growth curve experiments (Fig. 1b) were performed five times to ensure the reproducibility. Only mitochondrial aspect ratio was calculated based on one biological replicate (Fig. 4d), but multiple mitochondria were measured for each condition ( $n>80$ ). All microscopy findings were reliably reproduced. Data were analysed using GraphPad Prism 8 (GraphPad Software, La Jolla California USA). Values are presented as mean  $\pm$  standard deviation (SD). All the ratio data were log transformed as indicated prior to statistical analysis in GraphPad Prism and compared to 0 (uninfected/non-transfected/non-treated control) using one-way ANOVA with Tukey's multiple comparisons test (Fig. 1b, 6b and d), or Dunnett's multiple comparisons test (Fig. 4e-g, 5c, 6a, Extended Data Fig. 5c-d), Kruskal Wallis test with two-sided Dunn's multiple comparison test (Fig. 4d), two-tailed one-sample t-test (Fig. 5a), or two-way ANOVA and Sidak's multiple comparisons test (Fig. 5b and d). Statistical significance is indicated in the figures as follows: \*,  $p \leq 0.05$ ; \*\*,  $p \leq 0.01$ ; \*\*\*,  $p \leq 0.001$ ; \*\*\*\*,  $p \leq 0.0001$ . The exact *p*-values are provided in Source data.

### Data availability

The authors declare that the data supporting the findings of this study are available within the paper and its supporting files, including source data. All relevant data, including further image data and

processed data are available by request from the corresponding authors, with the restriction of data that would compromise confidentiality of blood donors. Raw sequencing data have been deposited in SRA under the accession numbers SRR10279972-SRR10280067. Mapped data from the four *Candida* species can be mined and browsed at Candidamine ([candidamine.org](http://candidamine.org)) and gene read counts from all samples can be found in our GitHub page [https://github.com/Gabaldonlab/Host-pathogen\\_interactions](https://github.com/Gabaldonlab/Host-pathogen_interactions) along with data analysis scripts for results reproducibility. Publicly available datasets/databases used in the study are: Ensembl (<https://www.ensembl.org/index.html>, last accessed on 08/08/2017), RefSeq (<https://www.ncbi.nlm.nih.gov/refseq/>, last accessed on 09/08/2017), CGOB (<http://cgob.ucd.ie/>, last accessed on 09/08/2017), NCBI nt database (<https://www.ncbi.nlm.nih.gov/home/download/>, last accessed on 23/03/2018), Candida Genome Database (<http://www.candidagenome.org/>, last accessed on 17/08/2017), Genome-wide annotation for Human database (<https://bioconductor.org/packages/release/data/annotation/html/org.Hs.eg.db.html>, last accessed on 10/03/2020).

#### **Code availability**

All transcriptome data analysis results, including figures, Extended Data and supplementary materials are fully reproducible using the scripts provided at our GitHub page [https://github.com/Gabaldonlab/Host-pathogen\\_interactions](https://github.com/Gabaldonlab/Host-pathogen_interactions).

#### **Acknowledgements**

M.P., H.H., E.I.; J.O.P.; T.G., G.B. and B.H. received funding from the European Union Horizon 2020 research and innovation program under the Marie Skłodowska-Curie grant agreement No 642095 (OPATHY). B. H. further receives support from the Deutsche Forschungsgemeinschaft (DFG) within the Collaborative Research Centre (CRC)/Transregio 124 FungiNet (Project C1). M.S.G. was supported by the German Research Foundation (Deutsche Forschungsgemeinschaft - DFG) Emmy Noether Program (project no. 434385622 / GR 5617/1-1). We would like to thank Christine Kämnitz from the Electron Microscopy Center in Jena for sample preparation for TEM. Schematic models in Figures 4-6 were created with images adapted from Servier Medical Art by Servier. Original images are licensed under a Creative Commons Attribution 3.0 Unported License.

#### **Author contributions**

*M.P. and H.H. contributed equally to this work. M.P. performed all the laboratory experiments (except TEM), analysed the data, wrote the manuscript and prepared the figures. H.H. performed all bioinformatic analyses, wrote the manuscript and prepared the figures. E.I. and J.O.P.*

performed infection experiments for RNA-Seq and edited the manuscript. S.S.L. performed the growth curve and flow cytometry experiments and helped with mtDNA depletion setup, including data analysis. T.K. performed additional RT-qPCR experiments. S.Mü. and T.K. contributed to the additional mitochondrial phenotypic assays and data interpretation. E.S. and B.Q. performed TEM experiments, analysed the data, and edited the manuscript. M.S.G., S.Mo., S.B. and G.B designed experiments and edited the manuscript. B.H. and T.G. conceived and designed the study and wrote the manuscript.

#### Competing interests

The authors declare no competing interests.

#### FIGURE LEGENDS

**Fig. 1. Pathogenicity patterns of four *Candida* species in the *in vitro* vaginal epithelial infection model.** (a) Adhesion, determined as the percentage of *Candida* cells from the original inoculum that adhered to vaginal epithelial cells (ECs) at 1 hour post-infection (hpi); Invasion, determined as percentage of *Candida* cells that invaded into the vaginal ECs at 3 hpi; Hyphal length ( $\mu\text{m}$ ), recorded at 3 hpi; Necrotic damage, measured by quantification of lactate dehydrogenase (LDH) activity in the supernatant and presented as percentage respective to total lysis (maximum damage control) at 24 hpi. All values are presented as mean  $\pm$  SD of  $n=3$  independent *in vitro* infection experiments. (b) Generation times of *Candida* species in Yeast Extract–Peptone–Dextrose (YPD) or RPMI 1640 media (used for vaginal EC infections) measured in 24-hour growth curves. All values are presented as mean  $\pm$  SD of  $n=5$  independent experiments. No statistically significant difference in growth between the species in neither YPD nor RPMI was observed (one-way ANOVA with the Greenhouse–Geisser correction and Tukey’s multiple comparisons test). (c) Micrographs of *Candida* morphology at 3 hpi and confluent biofilms at 24 hpi on vaginal ECs. Micrographs are representative of  $n=3$  independent experiments with similar results.

**Fig. 2. Dynamics of transcriptomic changes of the four *Candida* species investigated in this study at different time points.** (a) *Candida* species transcriptome dynamics plots from RNA-Seq data based on  $\log_2$  fold changes of expression during the course of infection compared to *Candida* adapted to RPMI culture medium (time point 0). Each line corresponds to the relative fold change of expression levels of a single gene. Numbers on the plots indicate a number of differentially expressed (DE) genes ( $|\log_2 \text{fold change}| > 1.5$ ,  $p_{\text{adj}} < 0.01$ , up-regulated - red, down-regulated - blue). (b) Gene-Ontology (GO) term enrichment analysis of up-regulated genes (category "Biological

Process") in the four *Candida* species. The x-axis indicates the fungal species, y-axis indicates GO term. Only significant ( $p_{\text{adj}} < 0.05$ ) GO enrichments are shown. DE gene analyses were done using DESeq2 v. 1.26.0 and comparisons against time point 0 were done using the two-sided Wald test. GO enrichment analysis was done using clusterProfiler v. 3.14.3, which performs the hypergeometric test. Adjustments of  $p$ -values for DE gene and GO enrichment were done by Benjamini-Hochberg procedure. See the Supplementary file 9 for the full list of enriched GO terms for each species, time-point, up- or down-regulation, and GO category.

**Fig. 3. Transcriptome dynamics of vaginal epithelial cells upon exposure to four *Candida* species.** (a) Transcriptome dynamics plots from RNA-Seq data based on  $\log_2$  fold changes compared to time point 0. Each line corresponds to the relative fold change of expression levels of a single gene. Numbers on the plots indicate the number of differentially expressed (DE) genes ( $|\log_2 \text{fold change}| > 1.5$ ,  $p_{\text{adj}} < 0.01$ , up-regulated - red, down-regulated - blue). (b) Venn diagrams showing similarities and differences of human DE genes in response to *Candida* species. (c) Proportion between the shared DE genes and the total number of DE genes (top panel); and proportion between shared DE genes and the DE genes induced exclusively by each fungal species (bottom panel). (d) PCA biplot of all analysed human samples. Labels of the data points correspond to sample identifiers, where "reseq" indicates that the sample was sequenced more than once (see Supplementary table 1 for details). (e) GO term enrichment analysis for up-regulated genes (category "Biological Process") of the host at different time points. The x-axis indicates the infecting *Candida* species. Only significant ( $p_{\text{adj}} < 0.05$ ) GO enrichments are shown. DE gene analyses were done using DESeq2 v. 1.26.0 and comparisons against time point 0 were done using the two-sided Wald test. GO enrichment analysis was done using clusterProfiler v. 3.14.3, which performs the hypergeometric test. Adjustments of  $p$ -values for DE gene and GO enrichment were done by Benjamini-Hochberg procedure.

**Fig. 4. *Candida* species induce mitochondrial responses in vaginal epithelial cells (ECs).** (a) Expression of mitochondrial and interferon-stimulated genes with all four species in direct contact with ECs, with non-viable (n.v.) *Candida* cells, and in the transwell system. Data for infection in direct contact and with n.v. *Candida* cells were derived from RNA-Seq data ( $\log_2 \text{fold change} > 1.5$  for *C. albicans*, *C. glabrata*, and *C. parapsilosis*;  $\log_2 \text{fold change} > 1.3$  for infections with *C. tropicalis*), while transwell experiments were done additionally as  $n=3$  independent experiments and transcription levels were analysed using RT-qPCR. (b) Mitochondrial imaging by fluorescence microscopy using MitoTracker® Deep Red FM at 1 hour post-infection (hpi). Scale bars represent 50  $\mu\text{M}$ . (c) Transmission Electron Microscopy (TEM) analysis of mitochondria in uninfected and *C.*

*albicans*-infected ECs (1 and 3 hpi): loss of mitochondrial integrity in infected ECs (white arrows), mitochondria (black arrow) localizing around the invading hyphae of *C. albicans* (blue arrow) at 3 hpi. **(d)** Mitochondrial aspect ratio quantified by TEM at 1 hpi ( $n \geq 80$  mitochondria examined over one independent experiment). **(e)** Mitochondrial membrane potential change at 1 hpi, positive control CCCP 100  $\mu$ M. **(f)** Levels of mtROS production at 1 hpi, positive control antimycin 100  $\mu$ M. **(g)** Levels of mtDNA released into cytosol (qPCR) upon infection with *Candida* species at 6 hpi, positive control tunicamycin 10  $\mu$ M. **(h)** Schematic model of the events associated with mitochondrial dysfunctions resulting in mtROS production and mtDNA release. All data are derived from  $n=3$  independent experiments, unless indicated otherwise **((d))**. Representative microscopy images **((b-c))** were taken from  $n=3$  biological replicates and similar results were observed. All values are presented as mean  $\pm$  SD relative to the uninfected (-) control (dotted lines on **((d-g))**). Statistical significance is indicated as: \*,  $p \leq 0.05$ ; \*\*,  $p \leq 0.01$ ; \*\*\*,  $p \leq 0.001$ ; \*\*\*\*,  $p \leq 0.0001$  (Kruskal–Wallis test with two-sided Dunn’s multiple comparison **(d)** and one-way ANOVA with Dunnett’s multiple comparisons test **(e-g)**).

**Fig. 5. Role of mtDNA in the induction of type I interferon in vaginal epithelial cells (ECs).** **(a)** Depletion of mtDNA level by treatment of vaginal ECs with 2',3'-dideoxycytidine (ddC) for 6 days, measured by qPCR. **(b)** Relative expression (RT-qPCR) of selected Interferon-Stimulated Genes (ISGs) (*IFNB1*, *IFI6*, *RSAD2*, *OASL*, *IRF9*, *MX2*, *ISG15*, *ZBP1*, and *IFI44*) in *C. albicans*-infected, mtDNA-depleted ECs at 3 hours post-infection (hpi). **(c)** Relative expression (RT-qPCR) of selected ISGs upon the transfection of ECs with amplified mtDNA fragments at 6 h post-transfection. **(d)** Relative expression of selected ISGs (RT-qPCR) in ECs transfected with total DNA obtained from vaginal ECs with and without mtDNA depletion at 6 h post-transfection. **(e)** Schematic model of ISG expression induction by released mtDNA. All values are presented as mean  $\pm$  SD relative to the uninfected/non-transfected (-) control (dotted lines) of  $n=3$  independent experiments. Statistical significance is indicated as: \*,  $p \leq 0.05$ ; \*\*,  $p \leq 0.01$ ; \*\*\*,  $p \leq 0.001$ ; \*\*\*\*,  $p \leq 0.0001$  (two-tailed one sample t-test **((a))**, two-way ANOVA and Sidak's multiple comparisons test **((b)** and **(d))**, and one-way ANOVA with Dunnett’s multiple comparisons test **((c))**).

**Fig. 6. Type I IFN signalling increases epithelial resistance and suppress innate immune activation.** **(a)** Epithelial damage caused by *C. albicans* 24 hours post-infection (hpi) after RNA interference (RNAi) for selected Interferon-Stimulated Genes (*MX2*, *CMPK2*, *IFI6*). **(b)** Epithelial damage caused by *C. albicans* 24 hpi without and with 0.1 ng/ml of interferon- $\beta$  (IFN- $\beta$ ) and the additional of anti-interferon- $\alpha/\beta$  receptor (IFNAR) antibody. **(c)** Levels of interleukin(IL)-6, IL-1 $\beta$ , and IL-1 $\alpha$  secretion by neutrophils incubated with supernatants (SN) from infected epithelial cells

(EC) and by ECs infected with *Candida* species 24 hpi. **(d)** Levels of IL-8 secretion by infected ECs 24 hpi with or without the addition of anti-IFNAR antibody. **(e)** Levels of IL-8 secretion by neutrophils after 24 h incubation with supernatants from EC infections with or without the addition of an anti-IFNAR antibody. Control supernatants of *Candida* cells alone were included to ensure that the neutrophils respond to secretions of the epithelial cells rather than the fungus (blue bars). **(f)** Schematic model of the proposed role of type I IFN pathway in immune regulation and protection against *Candida* infection. All values are presented as mean  $\pm$  SD of n=3 independent experiments (except n=4 for IL-8 production by ECs upon *C. albicans* infection). Statistical significance is indicated as: \*,  $p \leq 0.05$ ; \*\*,  $p \leq 0.01$ ; \*\*\*\*,  $p \leq 0.0001$  (one-way ANOVA with Dunnett's multiple comparisons test **((a))** or Tukey's multiple comparisons test **((b) and (d))**); "calb" denotes *C. albicans*, "cglab" - *C. glabrata*, "cpar" - *C. parapsilosis*, "ctrop" - *C. tropicalis*.

**Extended Data Fig. 1. Overall experimental design of the current study.** **(a)** Schematic representation of the experimental design. Each *Candida* species was co-cultivated with host cells. Controls included samples at 0 and 24 h for both host and yeasts alone. At the indicated time points of infection, fungal and host RNAs were independently extracted and subsequently combined (pooled) at a 2:3 fungus-to-host ratio into one sample for library preparation and sequencing. Sequencing data were mapped to a concatenated host and fungal reference genome. **(b)** Schematic representation of the entire study including all samples. Each symbol corresponds to a sequenced sample (or technical replicates of the same sample). Host samples are depicted with circles; *Candida* samples are depicted with squares; the strategy for combining (pooling) human and fungal RNAs in the same sequencing library is shown with ovals surrounding the corresponding samples; technical replicates (i.e. the same sequencing library sequenced several times) are surrounded with dashed rectangles. Control samples are depicted in yellow; interacting host and fungal samples are depicted in blue; host samples interacting with non-viable fungal cells are depicted in purple. Each row indicates the samples for each human-yeast interaction experiment.

**Extended Data Fig. 2. Distinct patterns of transcriptome profiles of the four *Candida* species upon interaction with human epithelial cells.** **(a)** Distribution of fully shared, partially shared and species-specific differentially expressed (DE) genes across the course of infections. Numbers on bar plots indicate the percentage (%). **(b)** Venn diagrams of DE genes (only 1-to-1 orthologs) in four *Candida* species at each time point. **(c)** PCA biplot based on expression levels of orthologous genes across *Candida* species, demonstrating a species-specific stratification of transcriptomic profiles of the four fungal pathogens; Labels of the data points correspond to sample identifiers, where "reseq" indicates that the sample was sequenced more than once (see Supplementary table 1 for details).

876 **Extended Data Fig. 3. Comparison of orthologous gene content similarities between co-**  
 877 **expressed gene modules in different yeast species. (a)** Comparison of *C. albicans* modules  
 878 against modules of other species. **(b)** Comparison of *C. glabrata* modules against modules of other  
 879 species. **(c)** Comparison of *C. parapsilosis* modules against modules of other species. **(d)**  
 880 Comparison of *C. tropicalis* modules against modules of other species. Each box represents a  
 881 module of a given species (reference module); the title of a box represents the reference module  
 882 name. Each reference module is compared with all modules of other three species, and the modules  
 883 of other species with the highest similarity to the reference module are plotted with horizontal bars,  
 884 representing level of similarity (in %). Labels of the horizontal bars indicate <species  
 885 name>\_<module name>. “calb” denotes *C. albicans*, “cglab” - *C. glabrata*, “cpar” - *C.*  
 886 *parapsilosis*, “ctrop” - *C. tropicalis*. The level of similarity refers to the fraction (in %) of shared  
 887 one-to-one orthologous genes between two given modules, defined as the intersection of gene lists  
 888 of orthologs of two modules divided by the union of these gene lists.

889

890 **Extended Data Fig. 4. Infection-specific differentially expressed (DE) genes of *Candida***  
 891 **species. (a)** Venn diagrams indicating similarities and differences of fungal DE\* genes in culture  
 892 medium only (control) and in response to epithelial cells (infection). \*To identify infection-specific  
 893 genes with a higher stringency, we applied filters of  $|\log_2 \text{fold change}| > 0$  and  $p_{\text{adj}} < 0.01$ . For the  
 894 downstream analysis of identified genes, we used a filtering of  $|\log_2 \text{fold change}| > 1.5$  and  $p_{\text{adj}} < 0.01$   
 895 for consistency with other results. Differential expression analysis was done using DESeq2 v.  
 896 1.26.0 and comparisons against time point 0 were done using the two-sided Wald test. **(b)**  
 897 Distribution of infection-specific fungal genes across the studied *Candida* pathogens. Bar plots  
 898 demonstrate the distribution of partially shared, fully shared, and species-specific genes. Numbers  
 899 on bar plots indicate the percentage (%). Venn diagrams depict numbers of fully shared genes (1-to-  
 900 1 orthologs) across species.

901

902 **Extended Data Fig. 5. *Candida* species induce type I interferon signalling independently of**  
 903 **apoptosis.** The proportion of healthy, necrotic, and apoptotic vaginal epithelial cells (ECs) 3 and 24  
 904 hours post-infection (hpi) with *Candida* in **(a)** A431 vaginal ECs used throughout this study and **(b)**  
 905 primary vaginal ECs. Treatment with 1.2  $\mu\text{M}$  staurosporine was used as a positive control. **(c)**  
 906 Mitochondrial membrane potential change of primary vaginal ECs at 1 hpi, positive control CCCP  
 907 100  $\mu\text{M}$ . **(d)** Relative expression (RT-qPCR) of selected Interferon-Stimulated Genes (ISGs) in *C.*  
 908 *albicans*-infected ECs where apoptosis was induced with 1.2  $\mu\text{M}$  staurosporine at 3 hpi. All values

are presented as mean  $\pm$  SD of n=3 independent experiments. Statistical significance is indicated as: \*,  $p \leq 0.05$ ; \*\*\*,  $p \leq 0.001$ ; \*\*\*\*,  $p \leq 0.0001$  (one-way ANOVA with Dunnett's multiple comparisons test ((c-d)).; "calb" denotes *C. albicans*, "cglab" - *C. glabrata*, "cpar" - *C. parapsilosis*, "ctrop" - *C. tropicalis*.

**Extended Data Fig. 6. Human transcriptome profiles response to fungal damage.** (a) Levels of LDH release by epithelial cells upon the damage by four fungal pathogens 24 hpi. All values are presented as mean  $\pm$  SD of n=3 independent experiments. (b) PCA plot of human samples interacting with non-viable and viable fungal species, including *C. albicans ece1 $\Delta$ / $\Delta$* . The plot is obtained using the RUVg function of RUVseq with k=1 (see Extended Data Fig. 7 for plots with alternative k values). Labels of the data points correspond to sample identifiers, where "reseq" indicates that the sample was sequenced more than once (see Supplementary table 1 for details). "non-viable" indicates host samples interacting with non-viable fungal cells; "*ece1 $\Delta$ / $\Delta$* " indicates host samples interacting with *C. albicans ece1 $\Delta$ / $\Delta$* .

**Extended Data Fig. 7. Human transcriptome response assessed with different parameters of batch effect correction.** PCA plots of human samples interacting with fungal cells obtained using k = 0, 1, 2, 3 values of RUVseq package for batch effect correction. Labels of the data points correspond to sample identifiers, where "reseq" indicates that the sample was sequenced more than once (see Supplementary table 1 for details). "non-viable" indicates host samples interacting with non-viable fungal cells; "*ece1 $\Delta$ / $\Delta$* " indicates host samples interacting with *C. albicans ece1 $\Delta$ / $\Delta$* .

**Extended Data Fig. 8. Applied gating strategies across flow cytometry experiments for epithelial cells:** (a) A431 cells (linked to Fig. 4e) and (b) primary vaginal cells (linked to Extended Data Fig. 6c). First, 10<sup>4</sup> events were analyzed based on their side scatter area (SSC-A) vs. forward scatter area (FSC-A). For further analysis, single cells were selected based on forward scatter height (FSC-H) vs. forward scatter area (FSC-A). MitoTracker® Deep Red FM signal was measured using detection channel Alexa 647-A. The unstained population was taken as a reference to determine the median fluoresce intensity of all samples (depicted as histogram Alexa 647-A- and Alexa 647-A+). The ratio from the median intensity of the stained/uninfected cells and unstained/uninfected cells was used as a reference to obtain the results of the infected samples shown in the manuscript figures.

## 944 REFERENCES

- 945 1 Mardh, P. A. *et al.* Facts and myths on recurrent vulvovaginal candidosis--a review on  
946 epidemiology, clinical manifestations, diagnosis, pathogenesis and therapy. *Int J STD AIDS*  
947 **13**, 522-539, doi:10.1258/095646202760159639 (2002).
- 948 2 Fidel, P. L., Jr. *et al.* An intravaginal live *Candida* challenge in humans leads to new  
949 hypotheses for the immunopathogenesis of vulvovaginal candidiasis. *Infect Immun* **72**,  
950 2939-2946, doi:10.1128/iai.72.5.2939-2946.2004 (2004).
- 951 3 Rosati, D., Bruno, M., Jaeger, M., Ten Oever, J. & Netea, M. G. Recurrent Vulvovaginal  
952 Candidiasis: An Immunological Perspective. *Microorganisms* **8**,  
953 doi:10.3390/microorganisms8020144 (2020).
- 954 4 Yano, J. *et al.* Current patient perspectives of vulvovaginal candidiasis: incidence,  
955 symptoms, management and post-treatment outcomes. *BMC Womens Health* **19**, 48,  
956 doi:10.1186/s12905-019-0748-8 (2019).
- 957 5 Makanjuola, O., Bongomin, F. & Fayemiwo, S. A. An Update on the Roles of Non-albicans  
958 *Candida* Species in Vulvovaginitis. *J Fungi (Basel)* **4**, doi:10.3390/jof4040121 (2018).
- 959 6 Gabaldon, T., Naranjo-Ortiz, M. A. & Marcet-Houben, M. Evolutionary genomics of yeast  
960 pathogens in the Saccharomycotina. *FEMS Yeast Res* **16**, doi:10.1093/femsyr/fow064  
961 (2016).
- 962 7 Consortium, O. & Gabaldon, T. Recent trends in molecular diagnostics of yeast infections:  
963 from PCR to NGS. *FEMS Microbiol Rev* **43**, 517-547, doi:10.1093/femsre/fuz015 (2019).
- 964 8 Meir, J. *et al.* Identification of *Candida albicans* regulatory genes governing mucosal  
965 infection. *Cell Microbiol* **20**, e12841, doi:10.1111/cmi.12841 (2018).
- 966 9 Verma, A., Gaffen, S. L. & Swidergall, M. Innate Immunity to Mucosal *Candida* Infections.  
967 *J Fungi (Basel)* **3**, doi:10.3390/jof3040060 (2017).
- 968 10 Moreno-Ruiz, E. *et al.* *Candida albicans* internalization by host cells is mediated by a  
969 clathrin-dependent mechanism. *Cell Microbiol* **11**, 1179-1189, doi:10.1111/j.1462-  
970 5822.2009.01319.x (2009).
- 971 11 Moyes, D. L. & Naglik, J. R. Mucosal immunity and *Candida albicans* infection. *Clin Dev*  
972 *Immunol* **2011**, 346307, doi:10.1155/2011/346307 (2011).
- 973 12 Moyes, D. L. *et al.* A biphasic innate immune MAPK response discriminates between the  
974 yeast and hyphal forms of *Candida albicans* in epithelial cells. *Cell Host Microbe* **8**, 225-  
975 235, doi:10.1016/j.chom.2010.08.002 (2010).
- 976 13 Naglik, J. R. & Moyes, D. Epithelial cell innate response to *Candida albicans*. *Adv Dent Res*  
977 **23**, 50-55, doi:10.1177/0022034511399285 (2011).
- 978 14 Naglik, J. R., Moyes, D. L., Wachtler, B. & Hube, B. *Candida albicans* interactions with  
979 epithelial cells and mucosal immunity. *Microbes Infect* **13**, 963-976,  
980 doi:10.1016/j.micinf.2011.06.009 (2011).
- 981 15 Zhu, W. & Filler, S. G. Interactions of *Candida albicans* with epithelial cells. *Cell Microbiol*  
982 **12**, 273-282, doi:10.1111/j.1462-5822.2009.01412.x (2010).
- 983 16 Westermann, A. J., Gorski, S. A. & Vogel, J. Dual RNA-seq of pathogen and host. *Nat Rev*  
984 *Microbiol* **10**, 618-630, doi:10.1038/nrmicro2852 (2012).
- 985 17 Hovhannisyan, H. & Gabaldon, T. Transcriptome Sequencing Approaches to Elucidate  
986 Host-Microbe Interactions in Opportunistic Human Fungal Pathogens. *Curr Top Microbiol*  
987 *Immunol* **422**, 193-235, doi:10.1007/82\_2018\_122 (2019).
- 988 18 Amorim-Vaz, S. *et al.* RNA Enrichment Method for Quantitative Transcriptional Analysis  
989 of Pathogens In Vivo Applied to the Fungus *Candida albicans*. *MBio* **6**, e00942-00915,  
990 doi:10.1128/mBio.00942-15 (2015).
- 991 19 Bruno, V. M. *et al.* Transcriptomic analysis of vulvovaginal candidiasis identifies a role for  
992 the NLRP3 inflammasome. *MBio* **6**, doi:10.1128/mBio.00182-15 (2015).
- 993 20 Liu, Y. *et al.* New signaling pathways govern the host response to *C. albicans* infection in  
994 various niches. *Genome Res* **25**, 679-689, doi:10.1101/gr.187427.114 (2015).
- 995 21 Tierney, L. *et al.* An Interspecies Regulatory Network Inferred from Simultaneous RNA-seq

996 of *Candida albicans* Invading Innate Immune Cells. *Front Microbiol* **3**, 85,  
997 doi:10.3389/fmicb.2012.00085 (2012).

998 22 Toth, R. *et al.* Investigation of *Candida parapsilosis* virulence regulatory factors during host-  
999 pathogen interaction. *Sci Rep* **8**, 1346, doi:10.1038/s41598-018-19453-4 (2018).

1000 23 Kammer, P. *et al.* Survival Strategies of Pathogenic *Candida* Species in Human Blood Show  
1001 Independent and Specific Adaptations. *mBio* **11**, doi:10.1128/mBio.02435-20 (2020).

1002 24 Huang, G. *et al.* Bistable expression of WOR1, a master regulator of white-opaque  
1003 switching in *Candida albicans*. *Proc Natl Acad Sci U S A* **103**, 12813-12818,  
1004 doi:10.1073/pnas.0605270103 (2006).

1005 25 Richardson, J. P. *et al.* Candidalysin Drives Epithelial Signaling, Neutrophil Recruitment,  
1006 and Immunopathology at the Vaginal Mucosa. *Infect Immun* **86**, doi:10.1128/IAI.00645-17  
1007 (2018).

1008 26 Mills, E. L., Kelly, B. & O'Neill, L. A. J. Mitochondria are the powerhouses of immunity.  
1009 *Nat Immunol* **18**, 488-498, doi:10.1038/ni.3704 (2017).

1010 27 Mohanty, A., Tiwari-Pandey, R. & Pandey, N. R. Mitochondria: the indispensable players in  
1011 innate immunity and guardians of the inflammatory response. *J Cell Commun Signal* **13**,  
1012 303-318, doi:10.1007/s12079-019-00507-9 (2019).

1013 28 West, A. P. *et al.* Mitochondrial DNA stress primes the antiviral innate immune response.  
1014 *Nature* **520**, 553-557, doi:10.1038/nature14156 (2015).

1015 29 Pervolaraki, K. *et al.* Differential induction of interferon stimulated genes between type I  
1016 and type III interferons is independent of interferon receptor abundance. *PLoS Pathog* **14**,  
1017 e1007420, doi:10.1371/journal.ppat.1007420 (2018).

1018 30 Chen, Y., Zhou, Z. & Min, W. Mitochondria, Oxidative Stress and Innate Immunity. *Front*  
1019 *Physiol* **9**, 1487, doi:10.3389/fphys.2018.01487 (2018).

1020 31 Zhang, Q. *et al.* Circulating mitochondrial DAMPs cause inflammatory responses to injury.  
1021 *Nature* **464**, 104-107, doi:10.1038/nature08780 (2010).

1022 32 Fridman, J. S. & Lowe, S. W. Control of apoptosis by p53. *Oncogene* **22**, 9030-9040,  
1023 doi:10.1038/sj.onc.1207116 (2003).

1024 33 Schneider, W. M., Chevillotte, M. D. & Rice, C. M. Interferon-stimulated genes: a complex  
1025 web of host defenses. *Annu Rev Immunol* **32**, 513-545, doi:10.1146/annurev-immunol-  
1026 032713-120231 (2014).

1027 34 Smeeckens, S. P. *et al.* Functional genomics identifies type I interferon pathway as central for  
1028 host defense against *Candida albicans*. *Nat Commun* **4**, 1342, doi:10.1038/ncomms2343  
1029 (2013).

1030 35 El-Diwany, R. *et al.* CMPK2 and BCL-G are associated with type 1 interferon-induced HIV  
1031 restriction in humans. *Sci Adv* **4**, eaat0843, doi:10.1126/sciadv.aat0843 (2018).

1032 36 Sobel, J. D. *et al.* Vulvovaginal candidiasis: epidemiologic, diagnostic, and therapeutic  
1033 considerations. *Am J Obstet Gynecol* **178**, 203-211, doi:10.1016/s0002-9378(98)80001-x  
1034 (1998).

1035 37 Casadevall, A. & Pirofski, L. A. The damage-response framework of microbial  
1036 pathogenesis. *Nat Rev Microbiol* **1**, 17-24, doi:10.1038/nrmicro732 (2003).

1037 38 Jabra-Rizk, M. A. *et al.* *Candida albicans* Pathogenesis: Fitting within the Host-Microbe  
1038 Damage Response Framework. *Infect Immun* **84**, 2724-2739, doi:10.1128/IAI.00469-16  
1039 (2016).

1040 39 Pirofski, L. A. & Casadevall, A. The damage-response framework of microbial pathogenesis  
1041 and infectious diseases. *Adv Exp Med Biol* **635**, 135-146, doi:10.1007/978-0-387-09550-  
1042 9\_11 (2008).

1043 40 Moyes, D. L. *et al.* Candidalysin is a fungal peptide toxin critical for mucosal infection.  
1044 *Nature* **532**, 64-68, doi:10.1038/nature17625 (2016).

1045 41 Wilson, D., Naglik, J. R. & Hube, B. The Missing Link between *Candida albicans* Hyphal  
1046 Morphogenesis and Host Cell Damage. *PLoS Pathog* **12**, e1005867,  
1047 doi:10.1371/journal.ppat.1005867 (2016).

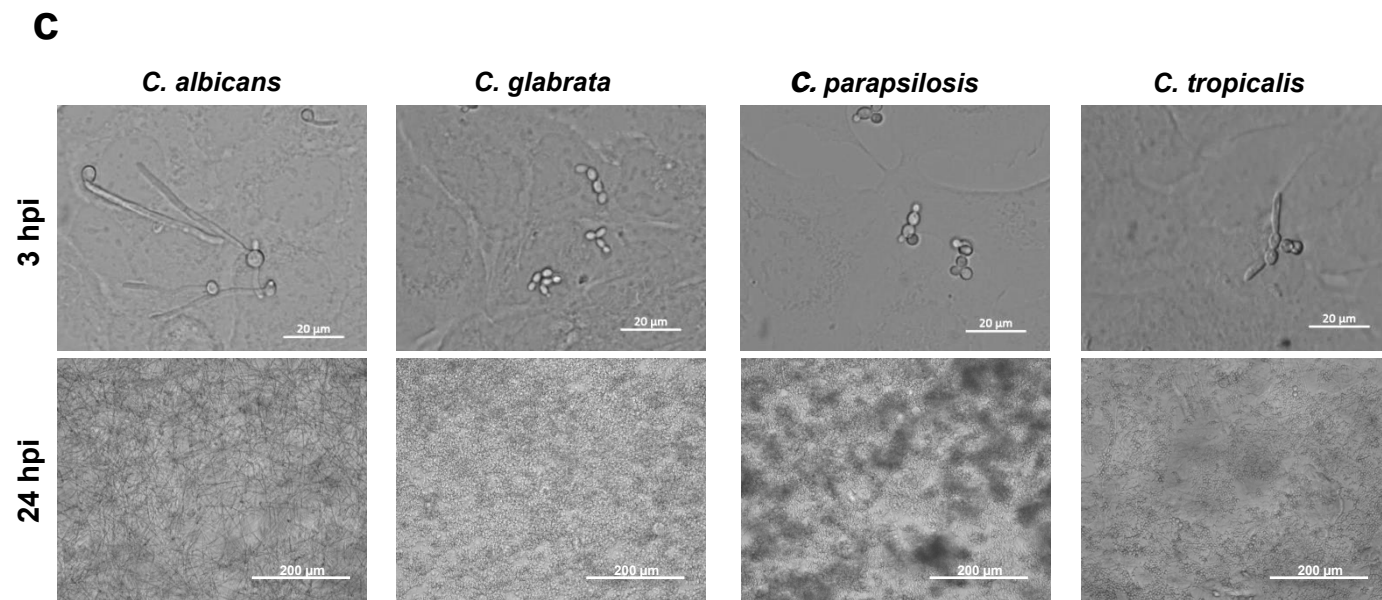
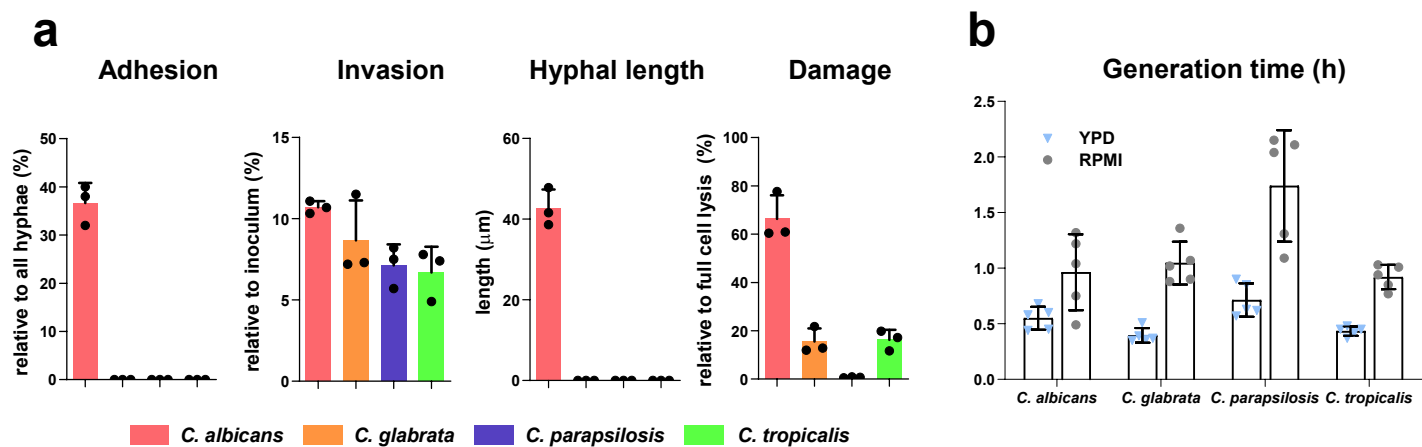
- 42 Kearney, C. J., Randall, K. L. & Oliaro, J. DOCK8 regulates signal transduction events to control immunity. *Cell Mol Immunol* **14**, 406-411, doi:10.1038/cmi.2017.9 (2017).
- 43 Chu, E. Y. *et al.* Cutaneous manifestations of DOCK8 deficiency syndrome. *Arch Dermatol* **148**, 79-84, doi:10.1001/archdermatol.2011.262 (2012).
- 44 McGhee, S. A. *et al.* DOCK8 Deletions and Mutations Are Associated With The Autosomal Recessive Hyper-IgE Phenotype. *Journal of Allergy and Clinical Immunology* **125**, AB356, doi:10.1016/j.jaci.2010.01.006 (2010).
- 45 Zhang, Q. *et al.* Combined immunodeficiency associated with DOCK8 mutations. *N Engl J Med* **361**, 2046-2055, doi:10.1056/NEJMoa0905506 (2009).
- 46 Isaacs, A. & Lindenmann, J. Virus interference. I. The interferon. *Proc R Soc Lond B Biol Sci* **147**, 258-267, doi:10.1098/rspb.1957.0048 (1957).
- 47 Riedelberger, M. *et al.* Type I Interferon Response Dysregulates Host Iron Homeostasis and Enhances *Candida glabrata* Infection. *Cell Host Microbe*, doi:10.1016/j.chom.2020.01.023 (2020).
- 48 Jaeger, M. *et al.* The RIG-I-like helicase receptor MDA5 (IFIH1) is involved in the host defense against *Candida* infections. *Eur J Clin Microbiol Infect Dis* **34**, 963-974, doi:10.1007/s10096-014-2309-2 (2015).
- 49 del Fresno, C. *et al.* Interferon-beta production via Dectin-1-Syk-IRF5 signaling in dendritic cells is crucial for immunity to *C. albicans*. *Immunity* **38**, 1176-1186, doi:10.1016/j.immuni.2013.05.010 (2013).
- 50 Kotredes, K. P., Thomas, B. & Gamero, A. M. The Protective Role of Type I Interferons in the Gastrointestinal Tract. *Front Immunol* **8**, 410, doi:10.3389/fimmu.2017.00410 (2017).
- 51 Munakata, K. *et al.* Importance of the interferon-alpha system in murine large intestine indicated by microarray analysis of commensal bacteria-induced immunological changes. *BMC Genomics* **9**, 192, doi:10.1186/1471-2164-9-192 (2008).
- 52 Sato, M. *et al.* Positive feedback regulation of type I IFN genes by the IFN-inducible transcription factor IRF-7. *FEBS Lett* **441**, 106-110, doi:10.1016/s0014-5793(98)01514-2 (1998).
- 53 Pekmezovic, M., Mogavero, S., Naglik, J. R. & Hube, B. Host-Pathogen Interactions during Female Genital Tract Infections. *Trends Microbiol* **27**, 982-996, doi:10.1016/j.tim.2019.07.006 (2019).
- 54 Li, T., Liu, Z., Zhang, X., Chen, X. & Wang, S. Therapeutic effectiveness of type I interferon in vulvovaginal candidiasis. *Microb Pathog* **134**, 103562, doi:10.1016/j.micpath.2019.103562 (2019).
- 55 Lirio, J. *et al.* Antifungal (oral and vaginal) therapy for recurrent vulvovaginal candidiasis: a systematic review protocol. *BMJ Open* **9**, e027489, doi:10.1136/bmjopen-2018-027489 (2019).
- 56 Grazioli, S. & Pugin, J. Mitochondrial Damage-Associated Molecular Patterns: From Inflammatory Signaling to Human Diseases. *Front Immunol* **9**, 832, doi:10.3389/fimmu.2018.00832 (2018).
- 57 Seth, R. B., Sun, L., Ea, C. K. & Chen, Z. J. Identification and characterization of MAVS, a mitochondrial antiviral signaling protein that activates NF-kappaB and IRF 3. *Cell* **122**, 669-682, doi:10.1016/j.cell.2005.08.012 (2005).
- 58 West, A. P. & Shadel, G. S. Mitochondrial DNA in innate immune responses and inflammatory pathology. *Nat Rev Immunol* **17**, 363-375, doi:10.1038/nri.2017.21 (2017).
- 59 Brokatzky, D. *et al.* A non-death function of the mitochondrial apoptosis apparatus in immunity. *EMBO J* **38**, doi:10.15252/emboj.2018100907 (2019).
- 60 Fang, C., Wei, X. & Wei, Y. Mitochondrial DNA in the regulation of innate immune responses. *Protein Cell* **7**, 11-16, doi:10.1007/s13238-015-0222-9 (2016).
- 61 Kim, E. S. *et al.* Mitochondrial dynamics regulate melanogenesis through proteasomal degradation of MITF via ROS-ERK activation. *Pigment Cell Melanoma Res* **27**, 1051-1062, doi:10.1111/pcmr.12298 (2014).

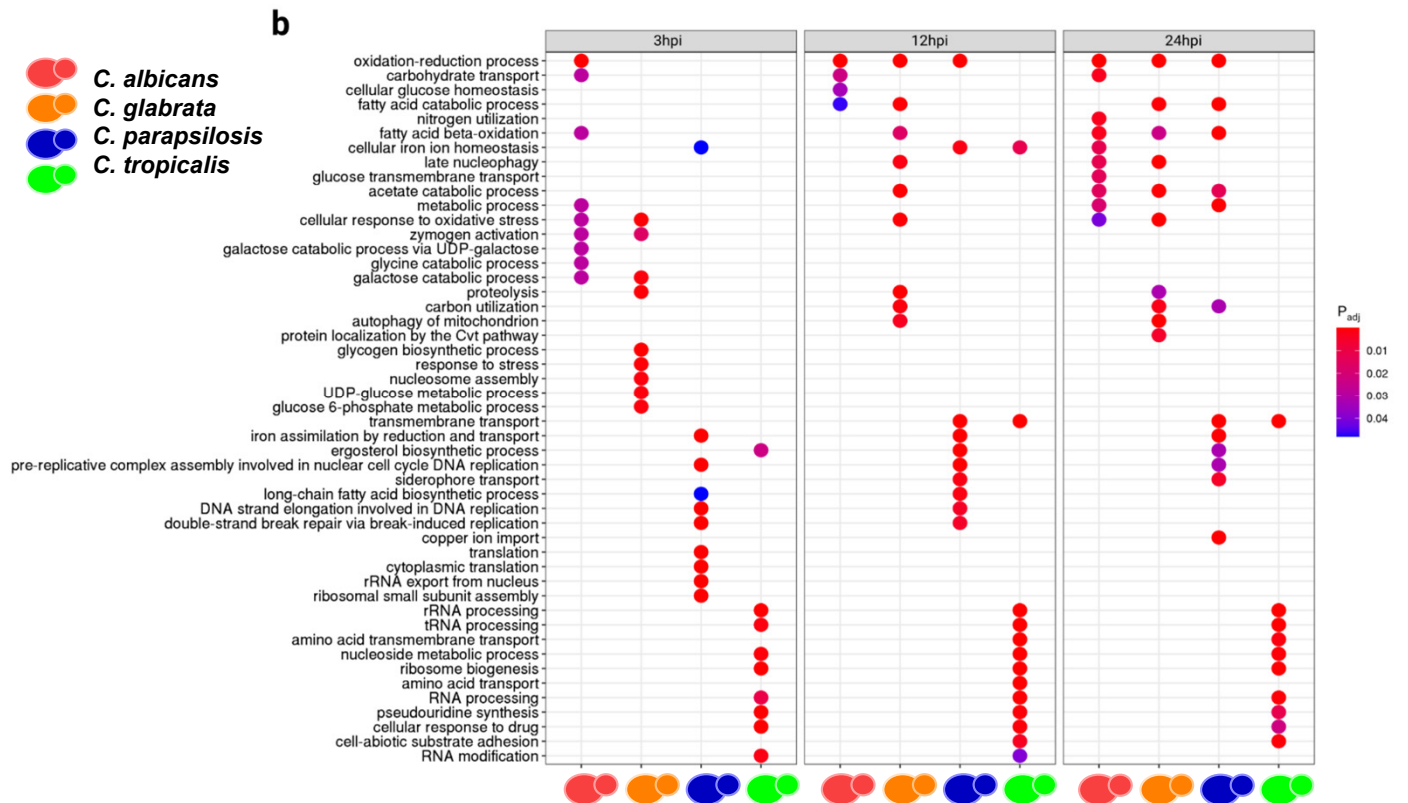
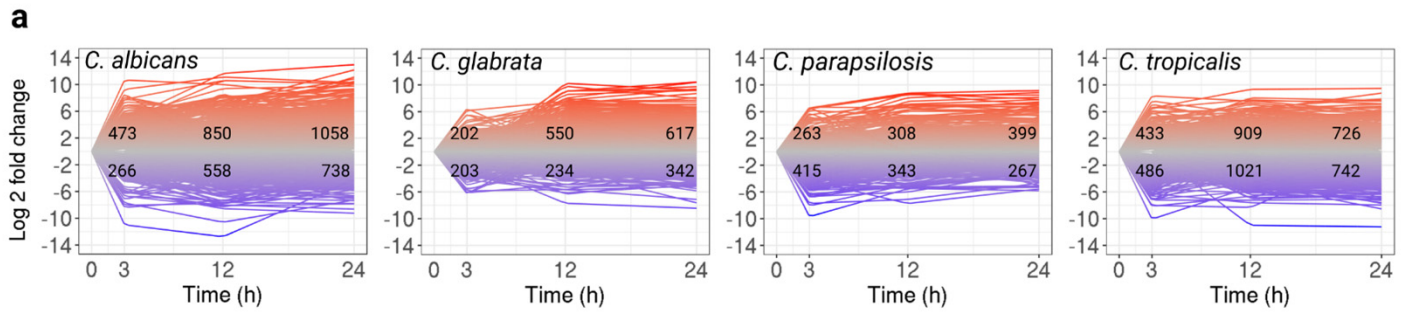
- 62 Plataki, M. *et al.* Mitochondrial Dysfunction in Aged Macrophages and Lung during Primary Streptococcus pneumoniae Infection is Improved with Pirfenidone. *Sci Rep* **9**, 971, doi:10.1038/s41598-018-37438-1 (2019).
- 63 Ramond, E., Jamet, A., Coureuil, M. & Charbit, A. Pivotal Role of Mitochondria in Macrophage Response to Bacterial Pathogens. *Front Immunol* **10**, 2461, doi:10.3389/fimmu.2019.02461 (2019).
- 64 West, A. P., Shadel, G. S. & Ghosh, S. Mitochondria in innate immune responses. *Nat Rev Immunol* **11**, 389-402, doi:10.1038/nri2975 (2011).
- 65 Kurihara, Y. *et al.* Chlamydia trachomatis targets mitochondrial dynamics to promote intracellular survival and proliferation. *Cell Microbiol* **21**, e12962, doi:10.1111/cmi.12962 (2019).
- 66 Kading, N. *et al.* Growth of Chlamydia pneumoniae Is Enhanced in Cells with Impaired Mitochondrial Function. *Front Cell Infect Microbiol* **7**, 499, doi:10.3389/fcimb.2017.00499 (2017).
- 67 Stavru, F., Bouillaud, F., Sartori, A., Ricquier, D. & Cossart, P. Listeria monocytogenes transiently alters mitochondrial dynamics during infection. *Proc Natl Acad Sci U S A* **108**, 3612-3617, doi:10.1073/pnas.1100126108 (2011).
- 68 Syn, G., Anderson, D., Blackwell, J. M. & Jamieson, S. E. Toxoplasma gondii Infection Is Associated with Mitochondrial Dysfunction in-Vitro. *Front Cell Infect Microbiol* **7**, 512, doi:10.3389/fcimb.2017.00512 (2017).
- 69 Gao, Y. *et al.* Mitochondrial DNA Leakage Caused by Streptococcus pneumoniae Hydrogen Peroxide Promotes Type I IFN Expression in Lung Cells. *Front Microbiol* **10**, 630, doi:10.3389/fmicb.2019.00630 (2019).
- 70 Wang, P. H. *et al.* A novel transcript isoform of STING that sequesters cGAMP and dominantly inhibits innate nucleic acid sensing. *Nucleic Acids Res* **46**, 4054-4071, doi:10.1093/nar/gky186 (2018).
- 71 Ning, X. *et al.* Apoptotic Caspases Suppress Type I Interferon Production via the Cleavage of cGAS, MAVS, and IRF3. *Mol Cell* **74**, 19-31 e17, doi:10.1016/j.molcel.2019.02.013 (2019).
- 72 Ichim, G. *et al.* Limited mitochondrial permeabilization causes DNA damage and genomic instability in the absence of cell death. *Mol Cell* **57**, 860-872, doi:10.1016/j.molcel.2015.01.018 (2015).
- 73 Gillum, A. M., Tsay, E. Y. & Kirsch, D. R. Isolation of the Candida albicans gene for orotidine-5'-phosphate decarboxylase by complementation of S. cerevisiae ura3 and E. coli pyrF mutations. *Mol Gen Genet* **198**, 179-182, doi:10.1007/bf00328721 (1984).
- 74 Tavanti, A., Davidson, A. D., Gow, N. A., Maiden, M. C. & Odds, F. C. Candida orthopsilosis and Candida metapsilosis spp. nov. to replace Candida parapsilosis groups II and III. *J Clin Microbiol* **43**, 284-292, doi:10.1128/JCM.43.1.284-292.2005 (2005).
- 75 Hernandez, R. & Rupp, S. Human epithelial model systems for the study of Candida infections in vitro: part II. Histologic methods for studying fungal invasion. *Methods Mol Biol* **470**, 105-123, doi:10.1007/978-1-59745-204-5\_10 (2009).
- 76 Schaller, M., Zakikhany, K., Naglik, J. R., Weindl, G. & Hube, B. Models of oral and vaginal candidiasis based on in vitro reconstituted human epithelia. *Nat Protoc* **1**, 2767-2773, doi:10.1038/nprot.2006.474 (2006).
- 77 Wachtler, B., Wilson, D., Haedicke, K., Dalle, F. & Hube, B. From attachment to damage: defined genes of Candida albicans mediate adhesion, invasion and damage during interaction with oral epithelial cells. *PLoS One* **6**, e17046, doi:10.1371/journal.pone.0017046 (2011).
- 78 Liu, Y., Zhou, J. & White, K. P. RNA-seq differential expression studies: more sequence or more replication? *Bioinformatics* **30**, 301-304, doi:10.1093/bioinformatics/btt688 (2014).
- 79 Chan, F. K., Moriwaki, K. & De Rosa, M. J. Detection of necrosis by release of lactate dehydrogenase activity. *Methods Mol Biol* **979**, 65-70, doi:10.1007/978-1-62703-290-2\_7

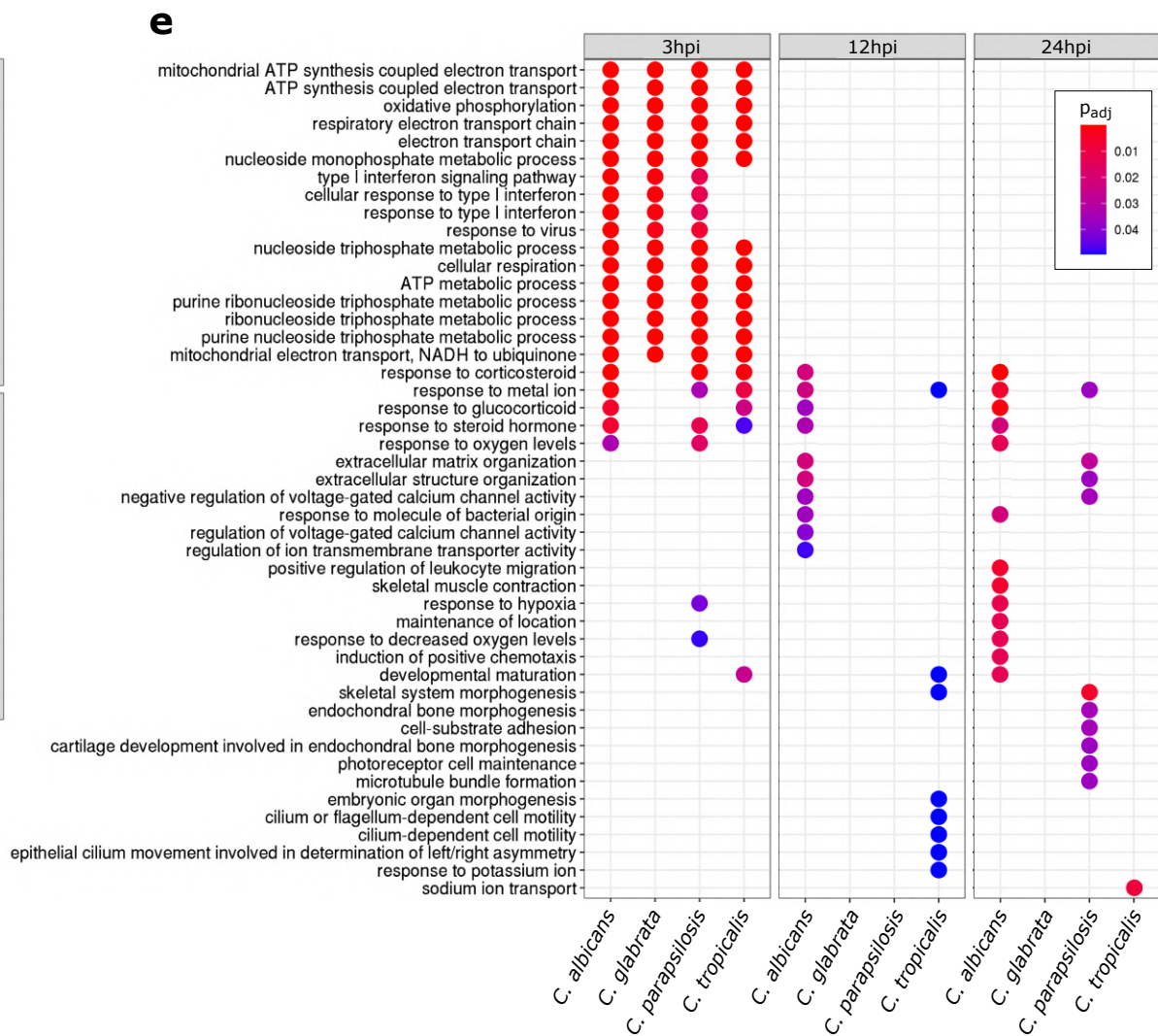
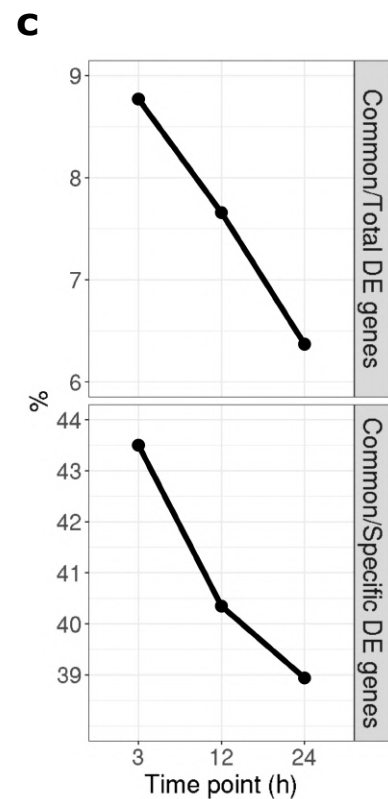
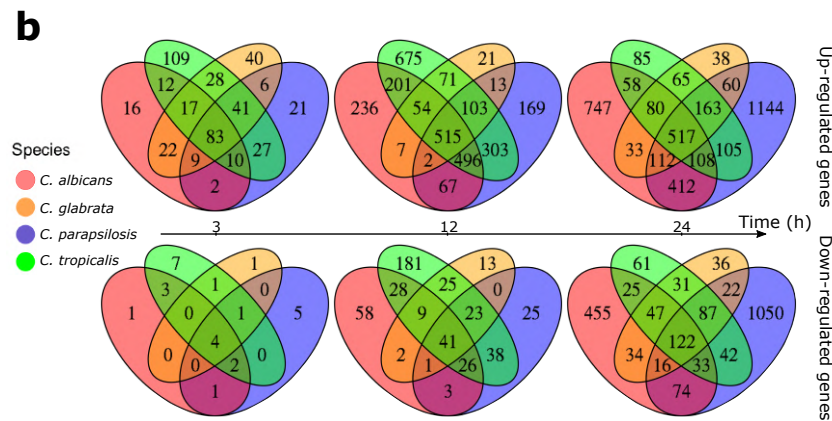
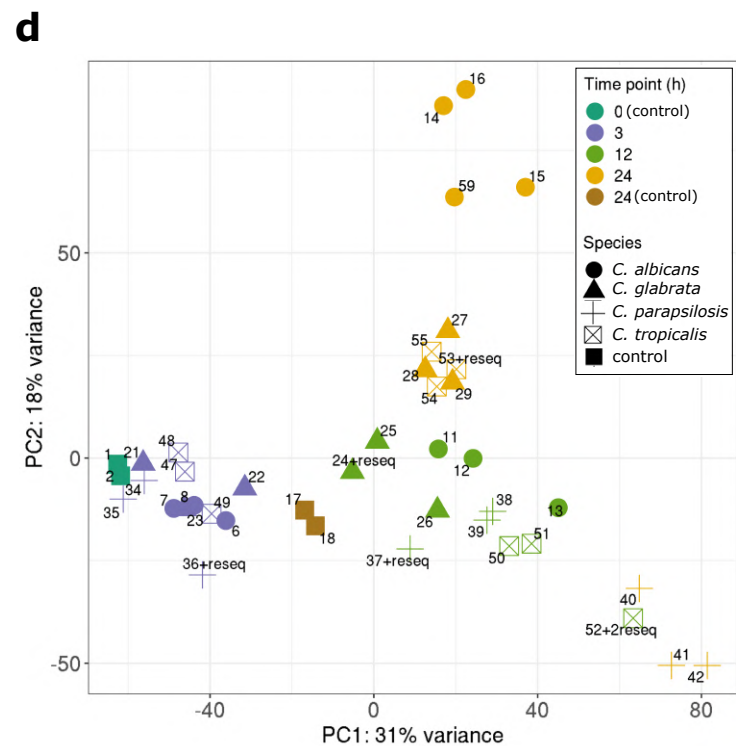
(2013).

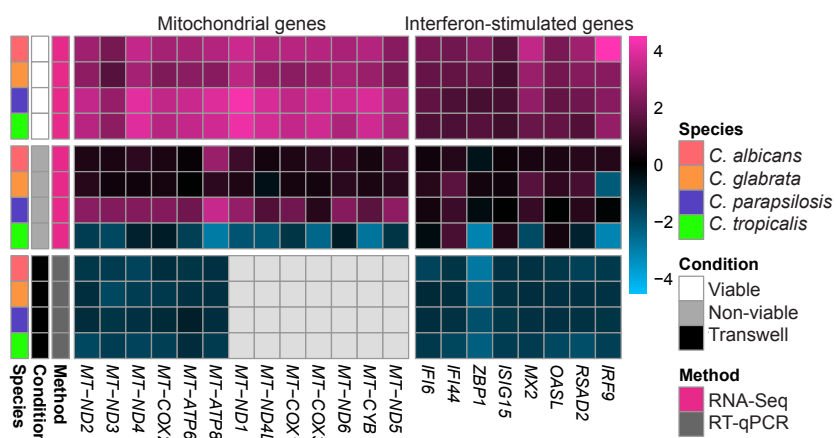
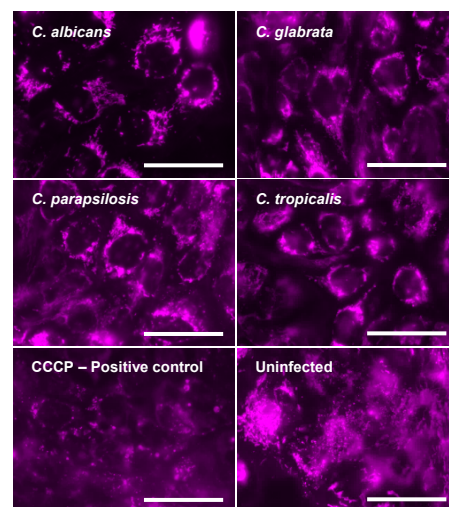
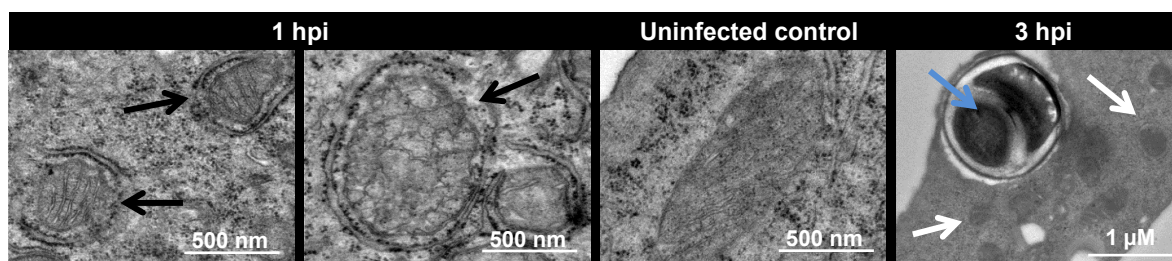
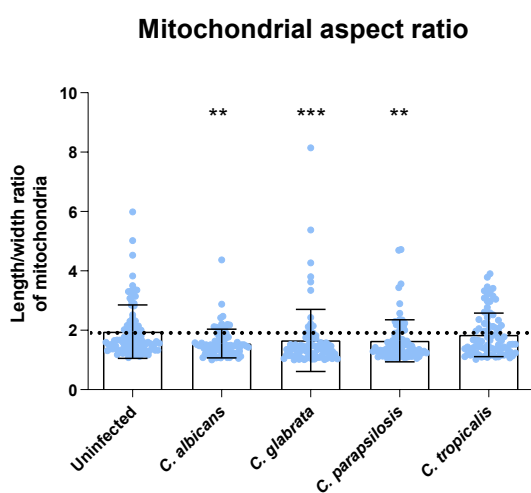
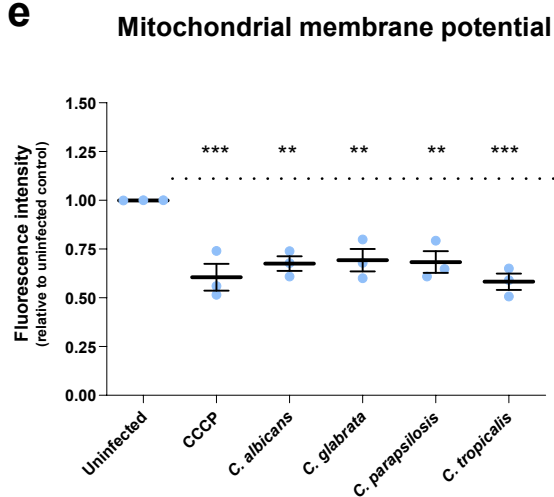
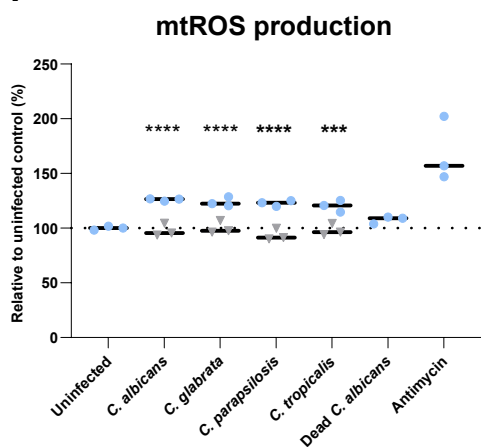
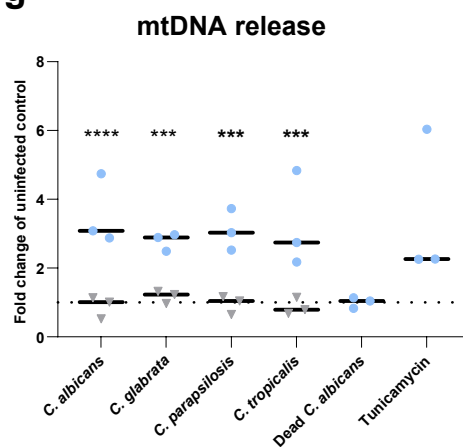
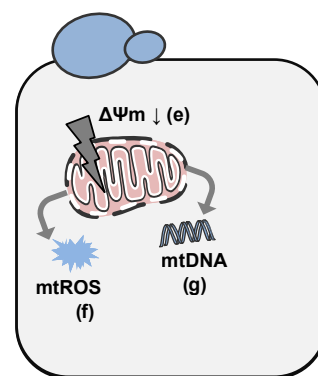
- 80 Bronner, D. N. & O'Riordan, M. X. Measurement of Mitochondrial DNA Release in Response to ER Stress. *Bio Protoc* **6**, doi:10.21769/BioProtoc.1839 (2016).
- 81 Win, S., Than, T. A., Fernandez-Checa, J. C. & Kaplowitz, N. JNK interaction with Sab mediates ER stress induced inhibition of mitochondrial respiration and cell death. *Cell Death Dis* **5**, e989, doi:10.1038/cddis.2013.522 (2014).
- 82 Bannwarth, S., Procaccio, V. & Paquis-Flucklinger, V. Rapid identification of unknown heteroplasmic mutations across the entire human mitochondrial genome with mismatch-specific Surveyor Nuclease. *Nat Protoc* **1**, 2037-2047, doi:10.1038/nprot.2006.318 (2006).
- 83 Gresnigt, M. S. *et al.* Neutrophil-mediated inhibition of proinflammatory cytokine responses. *J Immunol* **189**, 4806-4815, doi:10.4049/jimmunol.1103551 (2012).
- 84 Picard, M., White, K. & Turnbull, D. M. Mitochondrial morphology, topology, and membrane interactions in skeletal muscle: a quantitative three-dimensional electron microscopy study. *J Appl Physiol* (1985) **114**, 161-171, doi:10.1152/japplphysiol.01096.2012 (2013).
- 85 FastQC: a quality control tool for high throughput sequence data. Available online at: <http://www.bioinformatics.babraham.ac.uk/projects/fastqc> (2010).
- 86 Ewels, P., Magnusson, M., Lundin, S. & Kaller, M. MultiQC: summarize analysis results for multiple tools and samples in a single report. *Bioinformatics* **32**, 3047-3048, doi:10.1093/bioinformatics/btw354 (2016).
- 87 Bolger, A. M., Lohse, M. & Usadel, B. Trimmomatic: a flexible trimmer for Illumina sequence data. *Bioinformatics* **30**, 2114-2120, doi:10.1093/bioinformatics/btu170 (2014).
- 88 Dobin, A. *et al.* STAR: ultrafast universal RNA-seq aligner. *Bioinformatics* **29**, 15-21, doi:10.1093/bioinformatics/bts635 (2013).
- 89 Hunt, S. E. *et al.* Ensembl variation resources. *Database (Oxford)* **2018**, doi:10.1093/database/bay119 (2018).
- 90 Skrzypek, M. S. *et al.* The Candida Genome Database (CGD): incorporation of Assembly 22, systematic identifiers and visualization of high throughput sequencing data. *Nucleic Acids Res* **45**, D592-D596, doi:10.1093/nar/gkw924 (2017).
- 91 O'Leary, N. A. *et al.* Reference sequence (RefSeq) database at NCBI: current status, taxonomic expansion, and functional annotation. *Nucleic Acids Res* **44**, D733-745, doi:10.1093/nar/gkv1189 (2016).
- 92 Maguire, S. L. *et al.* Comparative genome analysis and gene finding in Candida species using CGOB. *Mol Biol Evol* **30**, 1281-1291, doi:10.1093/molbev/mst042 (2013).
- 93 Trapnell, C. *et al.* Transcript assembly and quantification by RNA-Seq reveals unannotated transcripts and isoform switching during cell differentiation. *Nat Biotechnol* **28**, 511-515, doi:10.1038/nbt.1621 (2010).
- 94 Kim, D., Song, L., Breitwieser, F. P. & Salzberg, S. L. Centrifuge: rapid and sensitive classification of metagenomic sequences. *Genome Res* **26**, 1721-1729, doi:10.1101/gr.210641.116 (2016).
- 95 Hovhannisyan, H., Hafez, A., Llorens, C. & Gabaldon, T. CROSSMAPPER: estimating cross-mapping rates and optimizing experimental design in multi-species sequencing studies. *Bioinformatics*, doi:10.1093/bioinformatics/btz626 (2019).
- 96 Love, M. I., Huber, W. & Anders, S. Moderated estimation of fold change and dispersion for RNA-seq data with DESeq2. *Genome Biol* **15**, 550, doi:10.1186/s13059-014-0550-8 (2014).
- 97 Risso, D., Ngai, J., Speed, T. P. & Dudoit, S. Normalization of RNA-seq data using factor analysis of control genes or samples. *Nat Biotechnol* **32**, 896-902, doi:10.1038/nbt.2931 (2014).
- 98 Yu, G., Wang, L. G., Han, Y. & He, Q. Y. clusterProfiler: an R package for comparing biological themes among gene clusters. *OMICS* **16**, 284-287, doi:10.1089/omi.2011.0118 (2012).

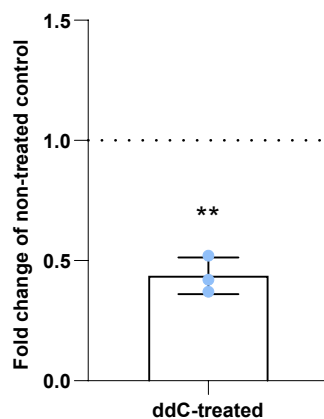
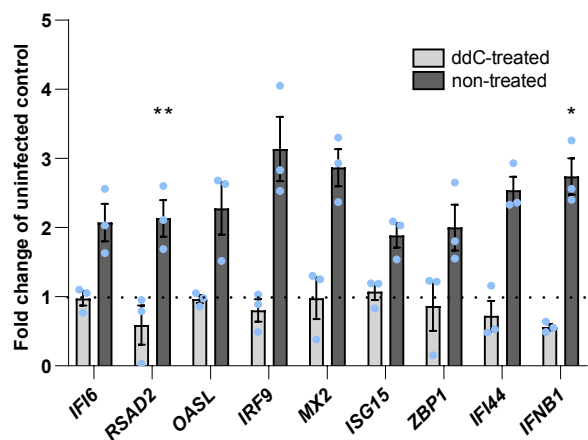
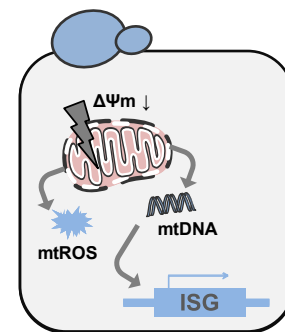
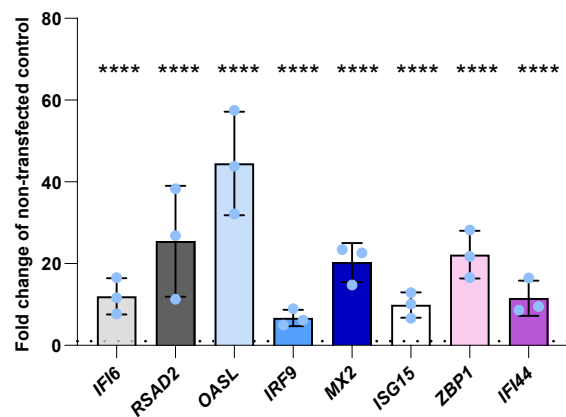
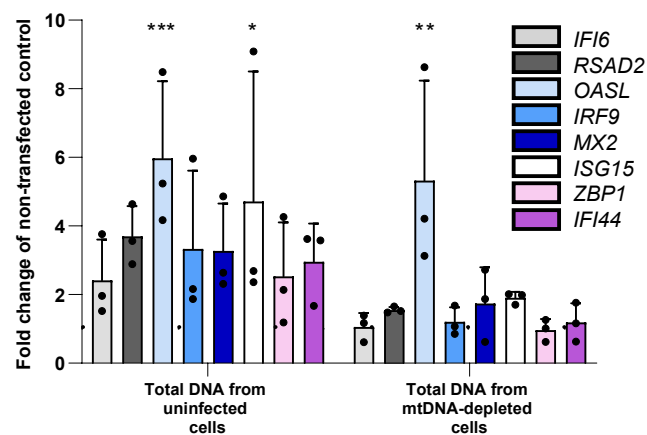
1204 99 org.Hs.eg.db: Genome wide annotation for Human. R package version 3.10.0 (2019).  
1205 100 Langfelder, P. & Horvath, S. WGCNA: an R package for weighted correlation network  
1206 analysis. *BMC Bioinformatics* **9**, 559, doi:10.1186/1471-2105-9-559 (2008).  
1207

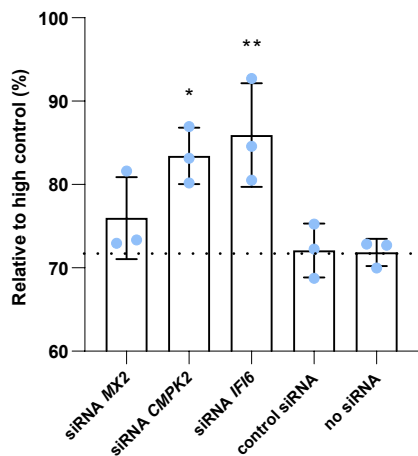
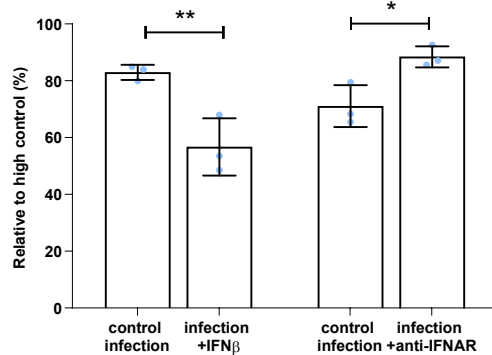
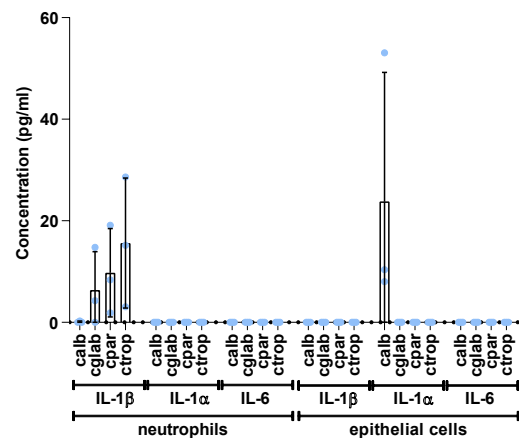
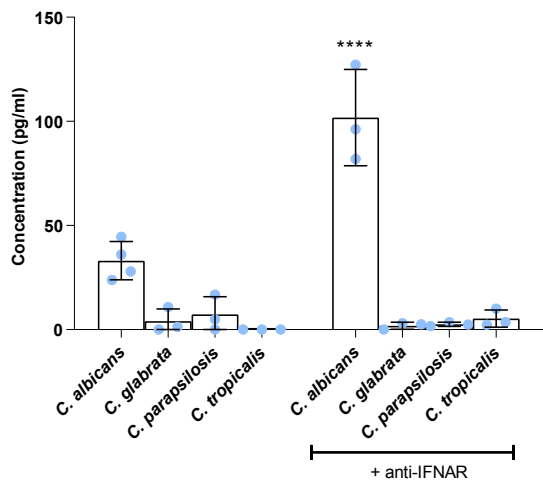
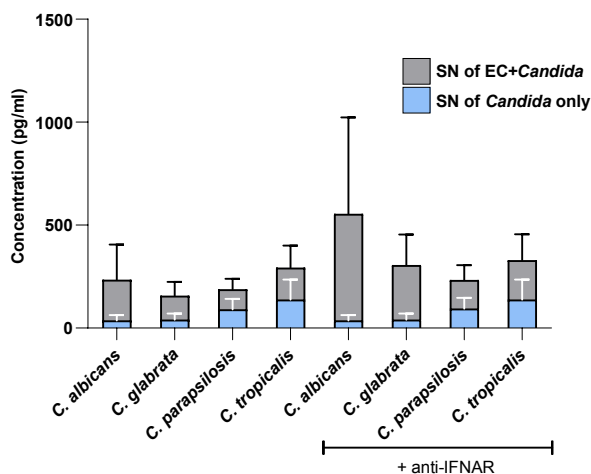






**a****b****c****d****e****f****g****h**

**a****mtDNA quantification****b****ISG expression upon *C. albicans* infection****e****c****ISG expression upon mtDNA transfection****d****ISG expression upon transfection**

**a****Epithelial damage****b****Epithelial damage****c****Other cytokines****d****IL-8  
vaginal epithelial cells****e****IL-8  
neutrophils****f**